Archives of Civil and Mechanical Engineering (2023) 23:219
https://doi.org/10.1007/s43452-023-00760-1

ORIGINAL ARTICLE

Pre- and post-heating mechanical properties of concrete containing recycled fine aggregate as partial replacement of natural sand and nano-silica as partial replacement of cement: experiments and predictions

Mohammad Asghari Shirvani[1] · Afshin Khodaparast[2] · Morteza Rezaeizadeh Herozi[3] · Reza Mousavi[4] · Saber Fallah-Valukolaee[4] · Amirhossein Ghorbanzadeh[4] · Mahdi Nematzadeh[4]

Received: 27 January 2023 / Revised: 13 July 2023 / Accepted: 16 July 2023 / Published online: 11 August 2023

Abstract
In this study, the effect of colloidal nano-silica replacing a fraction of cement and recycled concrete fine aggregate replacing natural sand on the post-fire mechanical features and durability of concrete was explored. To achieve this goal, 189 concrete samples were manufactured in total, with key variables being the volume of fine aggregate at 0, 50, and 100% replacing natural fine aggregate, the volume of nano-silica at 1.5, 3, 4.5, and 6% replacing the cement weight, and the exposure temperature at 20, 300, and 600 °C. Parameters selected for consideration in the concretes consisted of compressive capacity, splitting tensile capacity, elastic modulus, ultrasonic pulse velocity (UPV), and weight loss. Furthermore, using scanning electron microscopy (SEM) imaging, the microstructural condition of different sample groups was investigated. According to the findings, as the content of the recycled fine aggregate (RFA) replacing natural fine aggregate increased, the compressive capacity of the unheated and heated concretes declined, and the rate of this drop became greater as the replacement volume increased. On the other hand, the presence of the nano-silica and an increase in its content replacing the cement content in recycled aggregate concrete improved the compressive strength relative to the reference concrete for all the exposure temperatures, with the greatest improvement for the replacement percentage of 4.5%. In addition, the heat-induced compressive capacity drop was more pronounced at higher replacement levels of nano-silica. With a rise in the exposure temperature of the samples with only the recycled fine aggregate, fewer microcracks formed compared with the samples containing both recycled fine aggregate and nano-silica. The maximum weight loss occurred in the recycled sample containing the highest contents of nano-silica and recycled aggregate. Afterward, it was attempted to estimate the mechanical features of concrete by developing several empirical formulas as a function of temperature and volume fractions of recycled fine aggregate and nano-silica. These formulas were evaluated against the test data of this study and others, which showed an acceptable correlation. Finally, the findings of the tests were evaluated against the predictions of ACI 216, EN 1994–1-2, EN 1992–1-2, and ASCE.

Keywords Recycled fine aggregates · Nano-silica · Mechanical properties · High temperature · Prediction models · Concrete

✉ Mahdi Nematzadeh
m.nematzadeh@umz.ac.ir

[1] Department of Civil Engineering, Ayatollah Amoli Branch, Islamic Azad University, Amol, Iran

[2] Department of Earthquake Engineering, Faculty of Civil Engineering, University of Shahid Beheshti, Tehran, Iran

[3] Department of Civil Engineering, Iran University of Science and Technology, Tehran, Iran

[4] Department of Civil Engineering, Faculty of Engineering and Technology, University of Mazandaran, Babolsar, Iran

1 Introduction

1.1 Recycled concrete containing pozzolans

In recent years, construction practices have seen the application of the life cycle concept [1]. Several studies have addressed the need for research on the possibility of using recycled materials [2]. Because concrete structures have a short life and since natural disasters like floods, earthquakes, and storms frequently lead to the destruction of these structures, an increasing volume of concrete waste

is accumulating in landfills, leading to many problems for the environment [3]. Reusing old concrete waste in fresh concrete as recycled aggregates leads to the preservation of mineral resources, reduces the use of natural aggregates, protects the environment, lowers energy consumption, and cuts construction costs [4]. Recycled aggregates have old mortar stuck to them and thus, are generally less dense and resistant than natural aggregates, but their porosity is higher than natural aggregate [5]. Nevertheless, a number of researchers have explored the properties of recycled concrete aggregates. Solyman [6] reported that in comparison with natural fine aggregate (NFA), recycled fine aggregate (RFA) is more angular, irregular, and porous. Evangelista and De Brito [7] obtained higher values for the water absorption of RFA than NFA. The literature has shown that RFA is larger, more heterogeneous, and porous than NFA and has higher water absorption. Studies have also been done on the physic mechanical features of concrete with RFA. Solyman [6] demonstrated that the RFA quality affects the concrete compressive capacity, and the removal of mortar stuck to the primary natural aggregates in waste concrete can enhance the RFA quality. Also, according to the test results, the splitting tensile capacity of the samples declined by 19% at the RFA replacement percentage of 70%. Moreover, Nam, et al. [8] stated that the compressive and tensile capacities of RFAC were 10 and 26% less than concrete containing natural fine aggregate (NFA), respectively. Akono, et al. [9] studied the microstructure of concrete with RFA and reported that the porosity of C-S-H gel in RFA concrete was 56% of the total porosity. Pedro, et al. [10] observed that the compressive strength of recycled concrete compared to that of concrete containing natural aggregates declined by 5.4% (when 100% of natural aggregate was replaced with recycled aggregates), 10% (when 100% of natural fine grain was replaced with recycled fine grain) and 15% (when 100% of natural fine grain and coarse grain were replaced). This can be a useful solution to environmental problems due to the disposal of such waste. According to the above studies, using RFA in concrete lowers its the mechanical and physical features [11]. Thus, increasing the RFAC resistance is essential [12]. A number of strategies have been put forward to improve the capacity loss in RFAC, including an increase in the cement content and adding mineral additives [13]. Therefore, pozzolans can be used as cement additives to improve the mechanical and physical properties of concrete [14]. Using pozzolans to replace a fraction of the cement weight in recycled concretes improves the structure of concrete by enhancing the cement paste–aggregate interface transition zone (ITZ) [15]. This occurs as a result of the conversion of calcium hydroxide to calcium–silicate–hydrates gel (C-S–H) with the help of reactive silica, and also the reduction of the size and volume of weak calcium hydroxide (CH) crystals at the cement paste and aggregate interface [16]. Nowadays, practitioners working in the concrete technology field are becoming increasingly interested in using nanoparticles as new high-tech materials with minute particle sizes [17]. Nano-silica is one such material that increases the rate of the pozzolanic reaction and fills the nanometer-sized porosity of concrete because of its very small size and very high specific surface area relative to other pozzolanic materials [18]. Amin and Abu el-Hassan [19] explored how various nanomaterials affected mechanical properties of high-capacity concrete and found that substituting 3% of cement weight with nano-silica as the optimal volume fraction significantly improved the mechanical features of concrete. Palla, et al. [20] focused on the concrete mechanical features by adding 0.5–3% silica nanoparticles substituting for the cement waste at water/binder ratios of 0.23, 0.25, and 0.3. It was found that the mechanical features and durability of nano-silica-containing concrete improved by 20–30% compared to reference concrete. Sravanti and Sreeparvathy [21] examined how concrete capacity was affected by the incorporation of nano-silica. Nano-silica was used at 1, 2, 3, and 4% substituting for the cement weight. Their results showed that the addition of nano-silica increased the compressive and tensile capacity by 6–13% and 44–83%, respectively, with the highest amount of concrete containing 2% nano-silica.

1.2 Temperature

The load-carrying and mechanical characteristics of concrete elements will alter if a fire occurs in a structure as a possible phenomenon during its lifetime. To design and analyze nonlinear concrete members and study how the structure responds to high temperatures, it is necessary to assess the concrete mechanical features. Degradation of mechanical and physical properties and change in cracking behavior of heated concrete are caused by microcracks and internal stresses, and the decomposition of chemical compounds in cement paste [22]. In concrete, there is no sharp drop in capacity at temperatures below 300 °C; thus, through rehydration, the lost amount of capacity is partially restored, but if the temperature exceeds 300 °C, the high capacity of concrete is gone, and will not be restored [23]. The literature shows that recycled concrete has less cracking and less damage due to high porosity in the structure of concrete pores than ordinary concrete. In other words, the fire resistance in concretes containing recycled aggregate is higher than in ordinary concrete. This is because of the release of the water vapor pressure from the porosity of the recycled aggregate during the heating process, and the result is less damage to concrete [24]. Tanyildizi and Coskun [25] investigated the contribution of microsilica incorporation to the post-fire splitting tensile capacity and compressive capacity of lightweight concrete. According to the results, an increase in temperature lowered the compressive and tensile capacities

of the samples. Also, test results demonstrated that for all temperatures, the highest values of compressive and tensile capacities occurred in lightweight samples with 20% microsilica. Liu, et al. [26] explored the mechanical features of thermally insulated concrete incorporating recycled particles after experiencing high temperatures and reported that with a rise in temperature, the residual compressive capacity and elastic modulus of the concrete decreased significantly. However, the compressive capacity and elastic modulus values of concrete with recycled aggregate were always greater than conventional concrete. Baradaran-Nasiri and Nematzadeh [27] examined the impact of temperature on the durability and mechanical features of concrete containing recycled aggregate. Per the results, after passing the temperature of 800 °C, the samples containing recycled aggregate experienced a greater compressive capacity relative to the sample of ordinary concrete; thus, strength of the sample with 100% recycled particles was about twice that of the sample of normal concrete. Bui, et al. [28] investigated the effects of temperature on the mechanical features of samples incorporating recycled aggregate. It was reported that the heated recycled concretes had higher residual compressive capacity values compared with other samples at 20 °C.

2 Objective of present research

The increasing volume of municipal waste, especially from the demolition of buildings and worn-out urban fabric, has created many problems in large cities, and the recycling of this construction waste helps to protect the environment. On the other hand, extensive research has been done on the mechanical and physical features of recycled concrete containing pozzolans, while limited research is available on the effect of temperature on the durability and mechanical features of concrete containing recycled fine aggregate and nano-silica pozzolan. Thus, the objective of this work was to address the effect of RFA (0, 50, and 100% as volumetric substitutes for sand) and colloidal nano-silica (1.5, 3, 4.5, and 6% as weight substitutes for cement) on the post-heat mechanical features of recycled concrete (20, 300 and 600 °C). For this purpose, 189 concrete samples divided into 7 test groups were manufactured, and parameters consisting of the compressive capacity, pulse velocity, splitting tensile capacity, elastic modulus, and weight loss of samples were assessed. Then, it was attempted to predict the post-fire mechanical features of concrete with RFA and nano-silica by developing experimental formulas. Furthermore, the laboratory results for the mechanical features of heated concrete were compared with the predicted values of ACI 216, EN 1994–1-2, EN 1992-1-2, and ASCE. Finally, a microstructural analysis was performed to describe the microscopic properties of concrete components using SEM spectroscopy techniques.

The goals considered in the present research (innovation of the research) are as follows:

1. Evaluation of the post-heating mechanical properties of environmentally friendly concrete containing recycled fine aggregate as a partial replacement for natural sand and nano-silica as a partial replacement for cement.
2. Performing the ultrasonic pulse velocity (UPV) test in addition to the conventional mechanical tests (compressive strength, modulus of elasticity, tensile strength, etc.) and providing a prediction model for the compressive strength of heated and unheated concrete based on the UPV results.
3. Conducting scanning electron microscopy (SEM) imaging to evaluate the condition of the microstructure of heated and unheated concrete.
4. Determining the optimal percentage of nano-silica to replace cement in improving the mechanical properties of heated and unheated concrete.
5. Providing prediction models for different properties of heated concrete as a function of the studied variables. These models were proposed for parameters including compressive strength, tensile strength and modulus of elasticity. In order to confirm the models, the predicted values of the presented models were compared with the experimental results of the present research and other research.
6. The results of the mechanical properties of heated concrete were compared against the predictions of the common codes of practice including ACI 216, EN 1994–1-2, EN 1992–1-2, and ASCE.

3 Experimental study

3.1 Materials

Here, the coarse aggregate was crushed gravel with a max. nominal diameter of 12.5 mm and water absorption of 0.3%, and a density in saturated surface dry (SSD) mode of 2.68. Also, crushed sand in two recycled and natural states was used as fine aggregates with a modulus of softness of 3.1 and 2.8, specific density of 2.45 and 2.59 in SSD mode, water absorption of 8.6 and 1.9%, and the maximum nominal size of 4.75 mm, respectively. The percentage of aggregate passing through the sieves is shown in Table 1, and the gradation of the natural coarse, natural sand, and recycled sand is demonstrated in accordance with ASTM C33 [29] in Fig. 1. Type II Portland cement was used here with a density of 3.14, and also, nano-silica was used in different mixes

Table 1 Grading of aggregate

Sieve size	Fine agg.			Coarse agg.	
	Regulation limit (ASTM C33) Min–Max	Passing level (%)		Allowable limit (ASTM C33) Min–Max	Passing percentage (%)
		Sand agg	Recycled fine agg		
3/4 in. (19 mm)	100	–		100	100
1/2 in. (12.5 mm)	100	–		90–100	99
3/8 in. (9.5 mm)	100	100	100	40–70	66
No. 4 (4.75 mm)	95–100	99.28	100	0–15	3.4
No. 8 (2.36 mm)	80–100	86.5	94.6	0–5	1.15
No. 16 (1.18 mm)	50–85	67.58	55.42	–	–
No. 30 (0.6 mm)	25–60	43.16	29.43	–	–
No. 50 (0.3 mm)	5–30	19.42	13.28	–	–
No. 100 (0.15 mm)	0–10	2.34	0.34	–	–

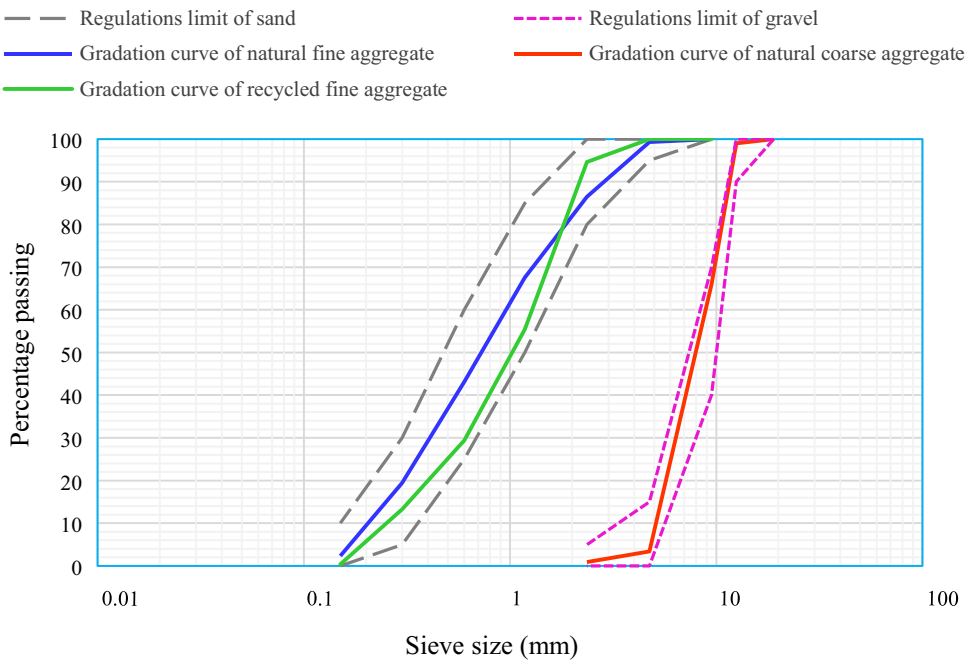

Fig. 1 Gradation of coarse and fine aggregate

with replacement ratios of 1.5, 3, 4.5, and 6% by weight of cement. The physicochemical features of nano-silica and cement are presented in Table 2. Here, to achieve concrete flowability of interest, a 3rd generation superplasticizer (SP) based on polycarboxylate ether with a density of 1.1 was poured into the mix to reach a high slump.

3.2 Mixing ratios and sample preparation

Mixing design ratios are presented in Table 3 per 1 m^3 of concrete based on ACI 211.1R [30]. In this study, 7 series of mixing schemes were considered with a water/cement ratio of 0.5. Here, different percentages of recycled sand were used separately and simultaneously with colloidal nano-silica in the concrete mix. To select experimental groups and concrete mixes, first, RFA with three different contents (0, 50, and 100%) was added to the concrete mix as a volume percentage of natural fine aggregate, leading to 3 mixing designs. Then, nano-silica pozzolan with 4 different percentages (1.5, 3, 4.5, and 6%) replacing cement weight was incorporated in mixes containing the highest content of recycled fine particles (100%), which resulted in 4 different mixing designs. Therefore, the number of considered mixing schemes reached seven.

The method of mixing the materials was in accordance with previous research [31, 32]. After the mixes were prepared, the slump test was performed per ASTM C143 [33] to determine the performance of fresh mixes, with the results

Table 2 Physicochemical properties of cementitious materials

Compound	Cementitious material (%)	
	Portland cement	Nano-silica
SiO_2	20.6	98.8
Al_2O_3	4.86	0.076
Fe_2O_3	3.37	0.293
CaO	63.56	0.392
MgO	2.18	0.05
SO_3	2.3	0.185
Na_2O	0.33	0.328
K_2O	0.54	0.08
TIO_2	–	0.064
P_2O_5	–	0.129
ZnO	–	0.021
CuO	–	0.02
Physical properties		
Specific gravity (gr/cm^3)	3.14	1.4
Specific surface (m^2/gr)	0.305	193
Initial setting time (min)	140	–
Final setting time (min)	190	–

Table 3 Concrete mix proportion

Mix ID	W/B	Mix proportions (kg/m^3)						SP (%)*	Slump (mm)
		Water	Cement	Nano- silica	Fine agg		Coarse agg		
					Recycled	Natural			
RFA0NS0	0.5	215	430	0	0	845.8	865.3	0	120
RFA50NS0	0.5	215	430	0	397.9	422.9	865.3	0	100
RFA100NS0	0.5	215	430	0	795.9	0	865.3	0	95
RFA100NS1.5	0.5	215	423.6	6.5	795.4	0	865.3	0.1	85
RFA100NS3	0.5	215	417.1	12.9	794.7	0	865.3	0.35	80
RFA100NS4.5	0.5	215	410.7	19.4	794.1	0	865.3	0.46	70
RFA100NS6	0.5	215	404.2	25.8	793.1	0	865.3	0.6	70

*Percentage of the total weight of cementitious material

listed in Table 3. The prepared concrete mixes were poured into molds and consolidated on a vibrating table. The samples were then demolded after 24 h and subjected to curing per ASTM C192 [34].

As Table 3 shows, RFA indicates the concrete samples containing the RFA, and the following number indicates the replacement percentage of the RFA with the natural fine aggregate. NS also represents nano-silica powder in the mix, and the following number gives the replacement level of this pozzolan for a fraction of the cement weight.

Here, 189 samples were fabricated to address the impact of several recycled fine nanoparticles and nano-silica contents on the durability and mechanical features of the samples having been exposed to high temperatures. Samples were in two sizes including 63 cube samples with a side length of 100 mm (21 samples in three groups) for compression, pulse velocity, and weight loss tests, as well as 126 cylindrical samples with dimensions of 150 × 300 mm, of which 63 (21samples in three categories) samples were for tensile capacity tests and 63 (21 samples of three series) samples were for testing the modulus of elasticity. Three

identical samples were considered for each test group to minimize errors and maximize reliability, and the reported results were the average values of these three samples. The manufacturing to testing procedure of the samples is provided in Fig. 2.

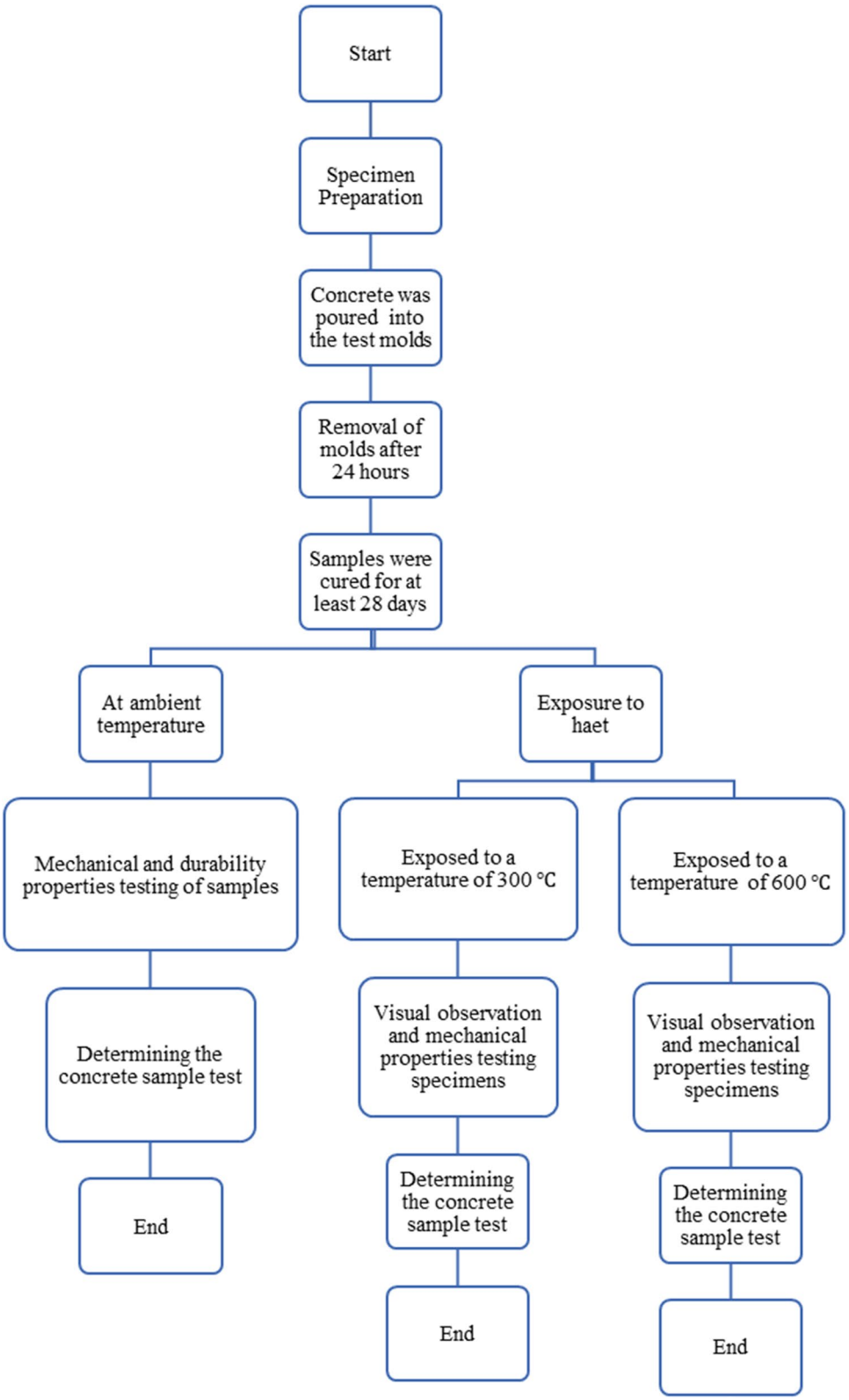

Fig.2 The process of concrete production to the testing

3.3 Exposure to heat

Prior to mechanical tests, each sample group was subjected to three thermal classes of 20, 300, and 600 °C, with the temperature of 20 °C considered as ambient temperature and others as high temperatures. All samples to be exposed to 300 and 600 °C were subjected to a pre-heating phase for 24 h at 60 °C in an electric oven until the surface became dry and potential spalling could be prevented [35]. The samples were placed in an electric furnace to be exposed to target temperatures according to the thermal pattern shown in Fig. 3, and after reaching the target temperature, they were continuously heated at the same temperature for one hour [36]. When the samples are exposed for greater than 1 h to a constant temperature, since the temperature at the center of the sample is closer to the furnace temperature, the outer surface of the sample is damaged more, particularly at 600 °C. When different intended temperatures were reached, the two furnace doors were slightly opened so that the samples could slowly cool down and become ready for tests. The samples remained outside the furnace for at least 7 days before the tests. Because concrete loses its physically and chemically bound water following heat treatment and experiences multiple cracks, it tends to absorb moisture in the air. This absorbed moisture functions as a rehydration agent, which leads to an increase in the volume of hydration products. This phenomenon applies lateral pressure on the cracks and increases their width, which in turn lowers the concrete capacity; therefore, it is necessary to leave the sample outside in the laboratory environment for seven days to further degrade the mechanical features of the concrete [37]. Figure 3a shows how the samples are placed inside the electric oven. The heating regime for heated concrete samples is shown in Fig. 3b.

3.4 Test procedures

In this study, the cubic 100 × 100 × 100 mm samples were subjected to the compression test at 28 days of age based on BS EN 12390 [38] with a 2000-kN compression tester at a loading rate of 0.3 MPa/sec. At the same time, the non-destructive ultrasonic pulse velocity (UPV) test was performed per ASTM C597 [39].

For this purpose, a non-destructive electronic ultrasonic machine accurate to 0.1 µs was applied to determine the ultrasonic pulse transmission time through direct transmission. Also, transducers with a vibration frequency of 54 kHz, an accuracy of ± 1% and ± 2% for distance, were used for travel time. Refractory grease was used to connect the transducers to a smooth surface of concrete. In each test on the samples, 5 measurements were made by changing the location of the transducers at the two opposite ends, and their average was calculated as the end result. When the laboratory transmission times were determined, the transmission speed of the ultrasonic pulse in the samples was obtained as the transmission distance (between the measured locations) divided by the transmission time. In addition, splitting tensile tests were carried out on the 150 × 300 mm cylindrical concrete samples after 28 days of curing using the same compression device in accordance with ASTM C496 [40] at a loading rate of 1.1 MPa/ min. On the other hand, ASTM C469 [41] can be employed to calculate the modulus of elasticity of the 150 × 300 mm cylindrical concrete samples. The weight loss test was also carried out on 100 mm cubic hardened samples after exposure to heat according to ISO 834 [42].

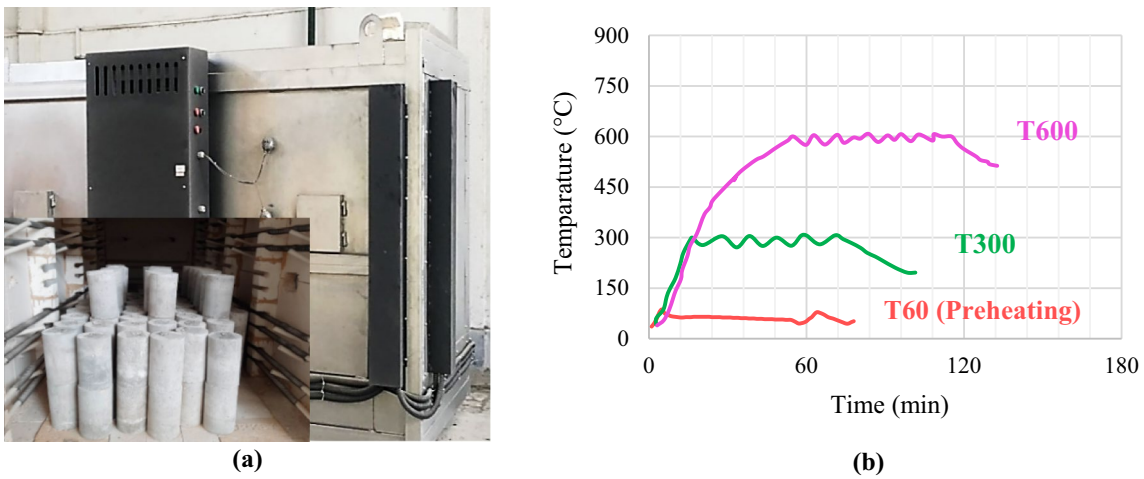

Fig. 3 **a** Placement of the samples in the furnace; **b** heating regime applied to the samples

4 Test results and discussion

4.1 Compressive capacity

The compressive capacity of the samples containing RFA and nano-silica is provided in Table 4 and Fig. 4. As can be seen in Table 4, the compressive capacity values of all unheated samples vary from 32.8 to 42.1 MPa. Moreover, from Fig. 4, it can be seen that substituting RFA for natural fine aggregate by 50 and 100% lowers the concrete compressive capacity by 9 and 21%, respectively; compared to the sample without recycled aggregate. The compressive capacity of recycled aggregate concrete declines due to the mortar adhering to these aggregates, which further weakens ITZ compared with conventional concrete (concrete with no recycled aggregates). In addition, high porosity, the presence of fine cracks, and the presence of dried mortar stuck to recycled aggregate lead to a lower concrete compressive capacity [33, 43].

On the other hand, adding nano-silica as a weight substitute for cement to concrete containing 100% RFA increases the compressive capacity relative to sample with no nano-silica. The reason for the improved capacity of sample incorporating nano-silica is a stronger bond between cement paste and aggregates and less porosity of the cement paste resulting from pozzolanic reactions [44]. Nano-silica makes the mortar in concrete denser by filling the porous space between the fine particles and the cement paste. Table 4 demonstrates that in concrete containing RFA, incorporating 1.5, 3, 4.5 and 6% nano-silica increases the compressive strength of the samples by 8.8, 17.7, 28.4 and 21.6%, respectively, compared to the concrete without pozzolan. Nanoparticles have a very high specific surface area, and thus, when their content exceeds a certain limit (optimal value), they can form cohesive and unstable lumps through a physical reaction, which reduces the concrete compressive capacity improvement [44]. However, since the water absorption of this pozzolan is high, incorporating it in large contents leads to an incomplete hydration reaction and reduced compressive strength (e.g., 6% nano-silica in this work).

With increasing the temperature, different concrete sample groups saw a considerable decline in their compressive capacity. For 300 °C, the compressive capacity of the reference sample (RFA0NS0) declined by 15.6% compared to that of the similar unheated sample. Also, concrete samples containing 50 and 100% RFA saw a decrease in capacity of 15.9 and 16.8% compared to the similar unheated sample.

Table 4 Test data of heated and non-heated concretes

Sample ID	Temperature (˚C)	Compressive capacity (MPa)		Splitting tensile capacity		Modulus of elasticity (GPa)		Ultrasonic pulse velocity (km/s)	Mass loss (%)
		Exp.	Pre.	Exp.	Pre.	Exp.	Pre.		
RFA0NS0 (R)	20	41.7	41.7	3.17	3.17	32.96	32.96	4.12	–
	300	35.2	34.6	2.61	2.60	22.88	24.58	3.57	3.1
	600	24.6	24.8	1.43	1.49	9.44	9.75	2.07	6.0
RFA50NS0	20	37.8	38.1	2.98	2.95	28.60	28.82	3.91	–
	300	31.8	31.6	2.46	2.42	21.50	21.50	3.38	4.5
	600	22.8	22.7	1.37	1.38	8.87	8.52	1.99	6.9
RFA100NS0	20	32.8	32.9	2.75	2.76	25.22	25.71	3.78	–
	300	27.3	27.3	2.31	2.26	19.56	19.17	3.24	5
	600	20.3	19.6	1.32	1.29	8.11	7.60	1.95	7.8
RFA100NS1.5	20	35.7	36.9	2.88	3.04	26.22	27.43	3.89	–
	300	29.4	30.6	2.41	2.49	20.68	20.46	3.44	5.3
	600	21.7	22.0	1.34	1.43	8.46	8.11	1.96	7.6
RFA100NS3	20	38.6	38.6	3.14	3.15	27.89	28.51	4.16	–
	300	31.8	32.0	2.61	2.59	21.70	21.26	3.70	4.8
	600	23.1	23.0	1.45	1.48	8.37	8.43	2.06	8.2
RFA100NS4.5	20	42.1	39.8	3.37	3.24	29.67	29.43	4.25	–
	300	34.4	33.0	2.82	2.65	22.82	21.95	3.85	4.4
	600	25.3	23.7	1.50	1.52	8.55	8.70	2.13	8.1
RFA100NS6	20	39.9	40.9	3.20	3.31	29.75	30.26	4.21	–
	300	32.2	33.9	2.67	2.71	21.87	22.57	3.77	4.7
	600	21.8	24.4	1.39	1.55	8.15	8.95	2.10	8.5

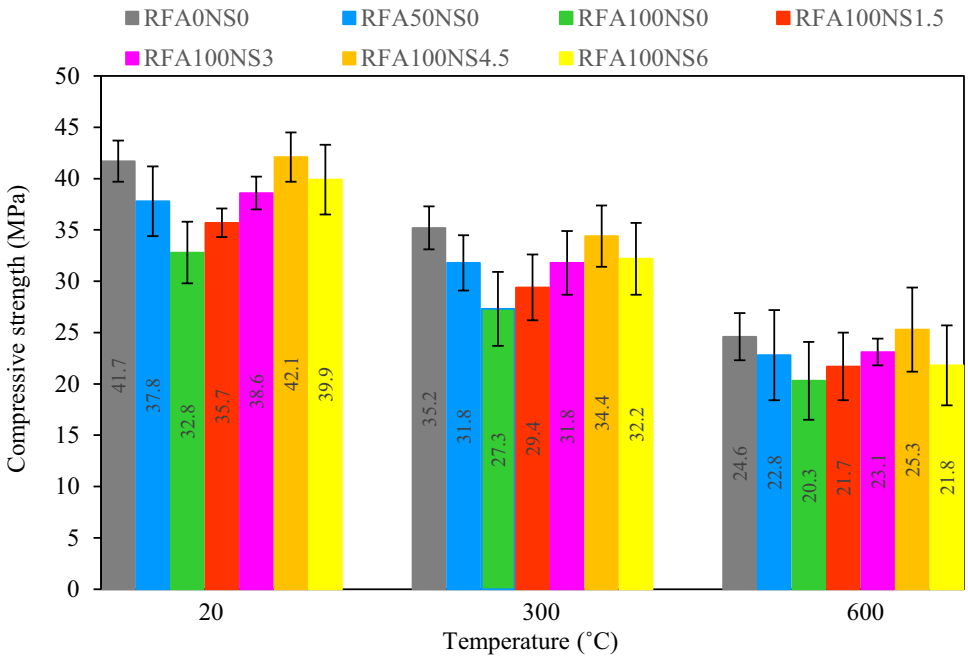

Fig.4 Compressive capacity of samples with RFA and nano-silica in terms of temperature

In general, the decrease in compressive capacity of samples at this temperature can result from the release of free water and chemical water in the C-S-H gel during exposure to heat, which leads to micro-cracks on the surface and internal stress and eventually capacity degradation [22, 45]. Furthermore, samples RFA100NS1.5, RFA100NS3, RFA100NS4.5, and RFA100NS6 saw decreases of 17.6, 17.6, 18.3, and 19.3%, respectively, in the compressive capacity relative to the similar unheated samples. Experimental studies have shown that concrete porosity is filled after pozzolans are added, creating denser concrete; the surface of this concrete is cracked and scaled due to high heat [46]. For 300 °C, as shown in Fig. 4, increasing the percentage of RFA lowered the compressive capacity of concrete relative to that of the reference concrete. This can originate from weak bonding between the recycled fine particles and the cement paste, in turn leading to a weakened ITZ. In addition, with a constant volume of RFA, as shown in Fig. 4, the compressive capacity improves by 7–26% as the percentage of nano-silica replacing the cement weight increased. At 600 °C, the compressive capacity of the samples dropped at a higher rate than other temperatures, such that the reference sample saw a compressive capacity reduction by 41% compared to the similar unheated sample. Moreover, samples RFA50NS0, RFA100NS0, RFA100NS1.5, RFA100NS3, RFA100NS4.5, and RFA100NS6 have a capacity reduction of 39.7, 38.1, 39.2, 40.2, 39.9, and 45.4%, respectively, compared to the corresponding unheated samples. The sharp drop in the capacity of the sample at this temperature occurs due to the decomposition and chemical evaporation of calcium hydroxide (CH) crystals, referred to as the dehydration phenomenon [35, 45]. The capacity loss after exposure to 600 °C compared to ambient temperature was between 38.1 and 45.4% for all concrete samples, with the lowest value for sample RFA100NS0. Normalized compressive capacity declined by incorporating nano-silica as a cement weight substitute because nano-silica fills the pores of the concrete structure and generates more compacted concrete. As a result, the water vapor pressure release due to heat is prevented and internal stresses increase, which ultimately leads to a decrease in bearing capacity.

Figure 5 demonstrates the fracture surface of the compressive test samples. In plain concrete without RFA, a regular and smooth fracture surface is seen, with cracks passing through the particles; however, at higher RFA volumes, the fracture surface becomes tortuous and irregular.

ITZ and the paste and the proximity of the aggregate resistance led to a reduction in the dimensions of the fracture process zone (FPZ) at the crack tip and also minimized the crack dimension. As shown in Fig. 5, a higher RFA volume increases the cement paste and ITZ porosity, in turn changing the failure mode from failure through particles to failure around them. Therefore, with increasing RFA replacement percentage, fractal dimensions increase.

The normalized compressive capacity is the compressive capacity after experiencing the temperature of interest, f_{cT}, divided by that at ambient temperature, f_c. Figure 6 provides the normalized compressive capacity values for the concrete samples per different temperatures. In addition, the normalized compressive capacity for heat-exposed concrete as proposed by ACI 216 [47], ASCE [48], and EN 1994-1-2 [49] is also provided in Fig. 6. This figure shows that

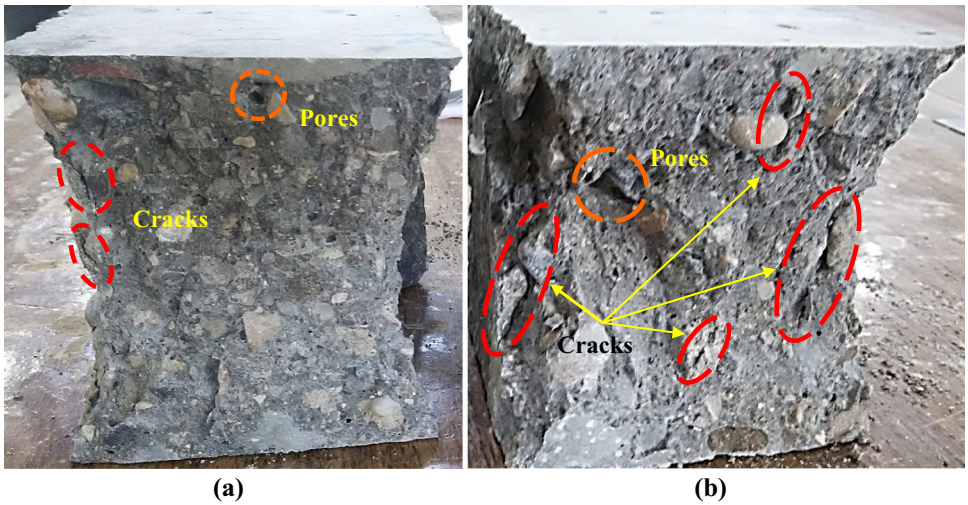

Fig. 5 Failure modes under compression load: **a** RFA0NS0, **b** RFA100NS0

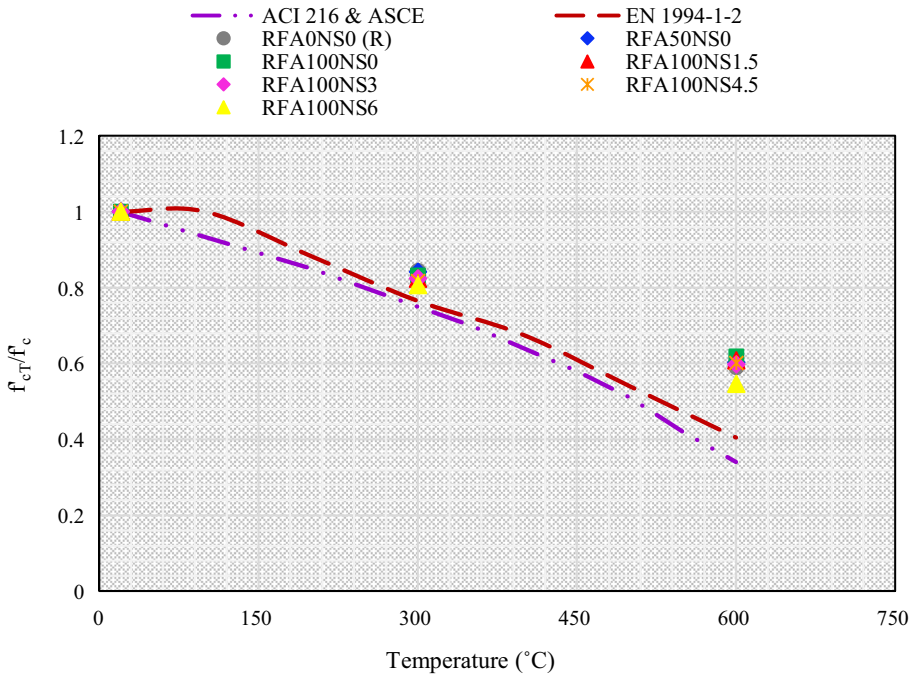

Fig.6 Normalized compressive capacity of samples per temperature

the provisions of [47–49] estimate the empirical data of the normalized capacity of all concrete samples with recycled fine nano-silica relatively well up to 300 °C, while at 600 °C, the normalized capacity of all samples is underestimated.

A relationship in the form of Eq. (1) was proposed by the nonlinear regression for predicting concrete compressive strength per parameters of temperature, volume of RFA, and weight percentage of nano-silica. This equation has a high coefficient of determination ($R^2 = 0.97$):

$$\frac{f_{cT}}{f_c} = \frac{f_{c(V_{RF},W_{NS},T)}}{f_{c(0,0,20)}} = \frac{1 - 0.21\ V_{RF}^{1.28} + 0.78\ W_{NS}^{0.5}}{1 + 1.66\ T'^{1.64}} \quad 0\% \leq V_{RF} \leq 100\%\ ,\ 0\% \leq W_{NS} \leq 6\%\ T' = \frac{T - 20}{1000}, \tag{1}$$

where T is the target temperature in degrees Celsius, T' is the temperature ratio, V_{RF} is the volume of RFA content and W_{NS} is the percentage of nano-silica replacement in concrete. To further evaluate and validate the proposed model (Eq. 1), the prediction results for compressive strength of concrete with RFA and nano-silica after exposure to laboratory results from other studies in the literature (Fallah and Nematzadeh

[44], Baradaran-Nasiri and Nematzadeh [27], Agarwal, et al. [50], Gao, et al. [51], Alhawat and Ashour [52], Yonggui, et al. [53] and Gao and Wang [13]) are compared in Fig. 7. Figure 7 shows that the results of the proposed compressive capacity model of concrete are in good agreement with the laboratory results of other researchers and the results of the present study. It should be noted that the combined effect of recycled fine granules and nano-silica on heat-exposed concrete samples was not found in the journals in order to study and compare with the experimental relationships obtained from the mechanical properties of the present study.

Figure 8 shows the response surfaces of the proposed model at three temperatures of 20, 300 and 600 °C. According to the figure, it is observed that by adding a percentage of RFA replacement, the compressive capacity of concrete is reduced, and in contrast, by adding nano-silica as a substitute for part of cement to concrete it is increased.

4.2 Ultrasonic pulse velocity

The mean values of ultrasonic pulse velocity (UPV) for heated and unheated concrete samples at different temperatures are presented in Table 4 and Fig. 9. In general, high levels of UPV are observed in higher-quality concrete. On the other hand, its low values indicate the volume of more cement products, as well as the presence of more pores and a greater distance between concrete particles. According to the concrete quality classification (based on UPV) provided in IS 1331.1-1 [54], four levels of excellent, good, medium and poor are defined, corresponding to $> 4.5, 3.5 \sim 4.5, 3.0 \sim 3.5, and < 3.0$, for which the UPV range is expressed in kilometers per second, respectively. Based on this classification, it is concluded that all concretes with different design ratios in this study are in good, medium and poor categories; thus, the quality of concrete mixtures according to the amount of UPV at high temperatures is reported as poor.

From the results, it can be seen that the amount of UPV decreases significantly with increasing temperature. The pulse velocity for reference concrete (RFA0NS0) was obtained as 4.12 km/s at ambient temperature. As the temperature reached 300 °C, the pulse rate of concrete sample RFA0NS0 decreased by 13.3% compared to ambient temperature and reached 3.57 km /s. The slow pulse rate of the samples at this temperature can be due to the escaping of pore water and limited chemical water in the C-S-H gel, which leads to a decrease in the integrity of the concrete matrix. With increasing temperature to 600 °C, the pulse speed of the concrete sample reached 2.07 km/s, showing a 49.8% decrease compared to the corresponding sample at ambient temperature. The reason for this sharp drop is the chemical decomposition of water in calcium hydroxide crystals and the significant decomposition of hydrated calcium silicate gel, which increases the voids in the cement paste and creates fine cracks in the transfer area [46, 55].

As the percentage of RFA replacement in concrete increased, the pulse velocity decreased significantly. The pulse velocities for samples RFA50NS0 and RFA100NS0 at 20 °C containing 50 and 100% RFA were 3.91 and

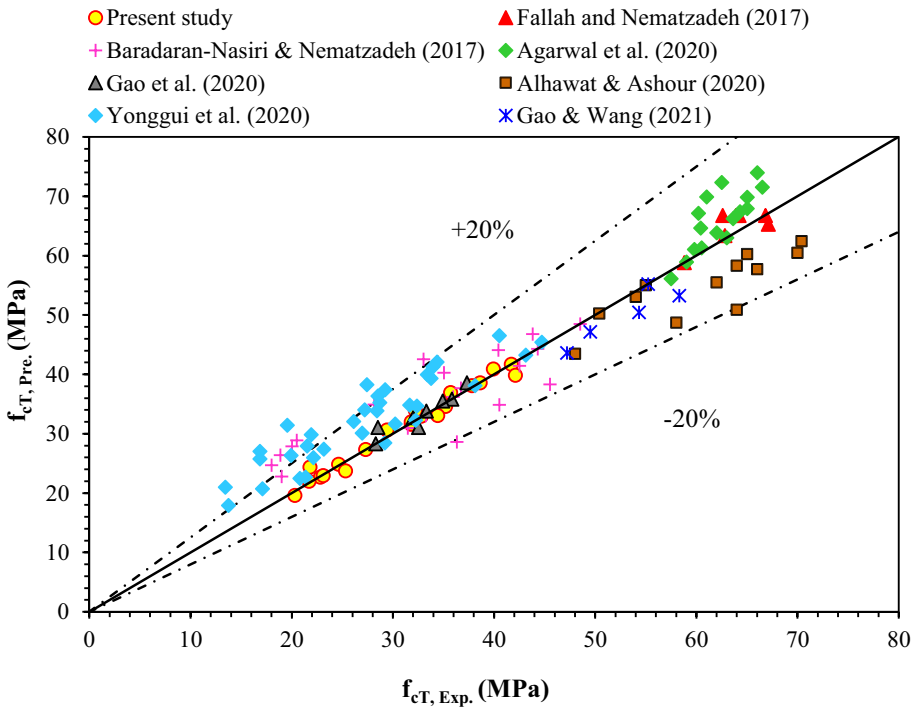

Fig. 7 Comparison of the results of the proposed compressive capacity model with the laboratory results of other researchers

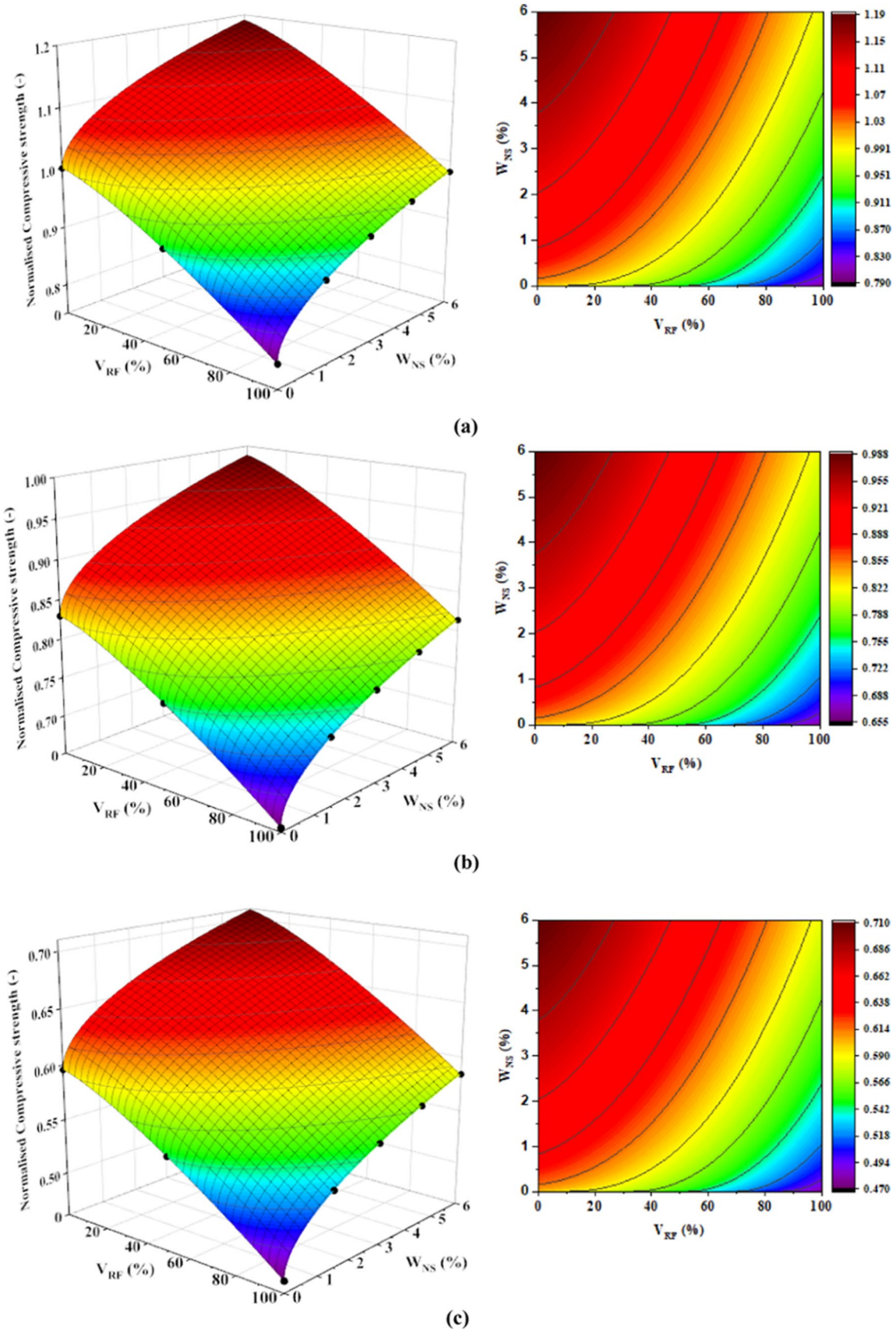

Fig. 8 Response surfaces of the proposed model for compressive capacity at different temperatures **a** 20 °C, **b** 300 °C, and **c** 600 °C

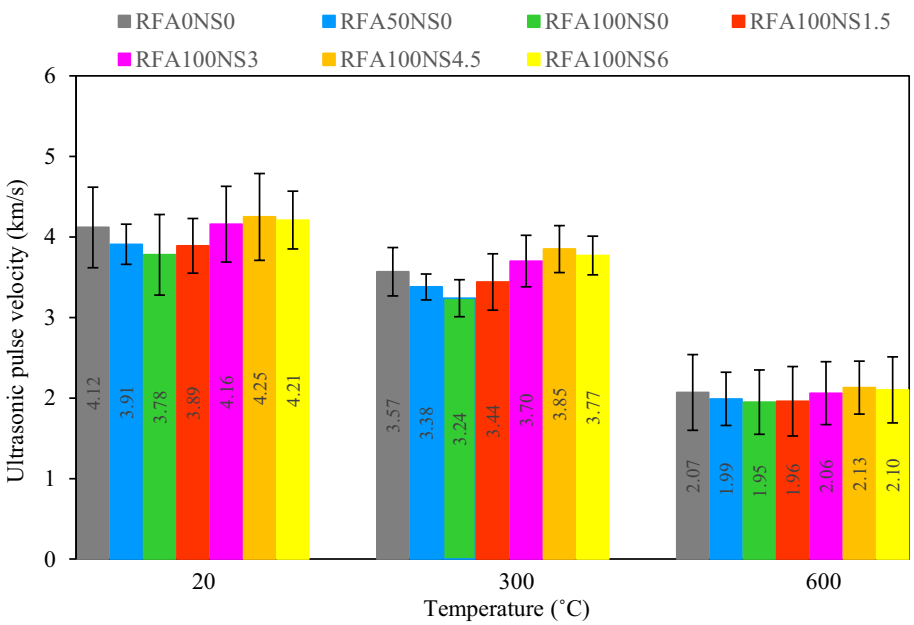

Fig.9 Ultrasonic pulse velocity of concrete samples exposed to high temperatures

3.78 km/s, respectively. There was a pulse drop of 5.1 and 8.3%, respectively, compared to the sample without recycled aggregate and nano-silica (RFA0NS0). The reduction can be due to high porosity, the presence of fine cracks, and the presence of dried mortar in recycled aggregate. On the other hand, the dried mortar around the aggregate particles causes a lack of proper adhesion between the recycled aggregates and the cement paste, which leads to a weak surface transfer zone in the concrete and reduces the velocity of the waves in the concrete. With increasing temperature to 600 °C, the pulse velocities of samples RFA50NS0 and RFA100NS0 experienced a drop of 49.1 and 48.4%, respectively, in comparison with ambient temperature, due to the decomposition of hydrated products in the cement paste (as mentioned in the previous section). On the other hand, the addition of recycled aggregates to the concrete mix causes water vapor to escape from the pores of the recycled aggregates during the heating process, leading to a greater capacity of the concrete.

On the other hand, Fig. 9 shows that the pulse velocity increases when nano-silica is incorporated into recycled aggregate concrete. The reason for the increase in the pulse velocity in concrete containing nano-silica is the improved bond between aggregates and cement paste [44, 56]. According to Table 4 and Fig. 9, in concretes containing RFA, the pulse velocity increased by 2.9, 10.1, 12.4 and 11.4% compared to the corresponding concrete without pozzolan (RFA100NS0) at ambient temperature when 1.5, 3, 4.5 and 6% nano-silica by cement weight are added. Nano-silica pozzolan enhances the recycled concrete structure and its concrete core consistency by reducing the size and amount of weak calcium hydroxide (CH) crystals present at the interface of cement paste and recycled aggregates, hence the pulse velocity of concrete with RFA increased with the increase of nano-silica as a weight substitute for cement. However, with increasing temperature and reaching 600 °C, the pulse velocity of RFA100NS1.5, RFA100NS3, RFA100NS4.5 and RFA100NS6 decreased by 49.6, 50.5, 49.9 and 50.1%, respectively, compared to the corresponding samples at ambient temperature. This shows that the rate of UPV drop in samples with different percentages of nano-silica at high temperatures is approximately equal. For 600 °C, the addition of nano-silica to the concrete mix fills the pores of the concrete structure and creates a denser concrete, which prevents the release of water vapor pressure due to heat, resulting in surface cracks in the concrete sample and spalling, which eventually leads to a significant drop in pulse velocity.

Ultrasonic pulse velocity test (UPV) is used as a non-destructive test to identify concrete integrity and concrete defects such as heterogeneity and the presence of cracks in the concrete volume, which are directly related to the compressive capacity of concrete. According to the passing pulse velocities and available strengths, the quadratic curve is the most suitable line passing through the desired points. There is no general relationship between the use of ultrasonic pulse velocity in estimating the compressive capacity of concrete. Many researchers [35, 57, 58] have shown that the relationship between compressive capacity and ultrasonic pulse velocity can be evaluated with a polynomial function; this relationship applies to samples containing recycled aggregates and concrete samples containing pozzolans. Mukharjee and Barai [58] also proposed a 2nd-degree curve for nano-silica recycled concrete.

However, some researchers have proposed an exponential function for estimating the compressive capacity of concrete using ultrasonic pulse velocities [59–61]. In this study, nonlinear regression analysis was used for laboratory results with a suitable quadratic function, Eq. (2), to determine the relationship between compressive capacity and UPV for concrete samples containing recycled fine nanoparticles and nano-silica after exposure to heat. It shows a suitable coefficient of determination ($R^2 = 0.94$), as can be seen in Fig. 10. From Fig. 10 and Eq. (2), it can be concluded that with an increase in the pulse velocity values in concrete, the compressive capacity increases:

$$f_c = 3.45\ V^2 - 13.35\ V + 35.6. \quad (2)$$

In the above, f_c and V are the compressive strength of concrete and the speed of ultrasonic pulse, in MPa and km/s, respectively.

Figure 11 shows a comparison of the results obtained from the developed model with results in the literature (Nematzadeh, et al. [35], Jain, et al. [57] and Sadrmomtazi, et al. [62]). As can be seen, the proposed model estimates the compressive capacity results of other researchers using pulse velocity well.

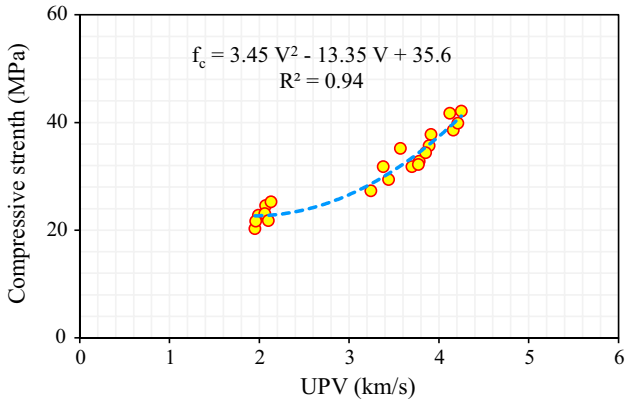

Fig.10 Experimental relationship between compressive capacity and UPV with laboratory data for all concrete samples exposed to high temperatures

4.3 Splitting tensile capacity

Table 4 and Fig. 12 provide the results of the splitting tensile capacity of concrete samples containing RFA and nano-silica exposed to high temperatures. According to Fig. 12, the tensile capacity of samples, like the compressive capacity, decreases with increasing the volume of RFA. At ambient temperature, the tensile capacity of the samples containing 50 and 100% RFA was 6 and 13.2% lower relative to the control concrete (RFA0NS0), respectively. The decrease in tensile capacity in concrete containing RFA results from the mortar adhering to the recycled aggregates acting as a separator between the other mix solid components, weakening the ITZ bond and resulting in stress concentration; this, in turn, leads to faster tensile failure [13, 32]. Rao [63] also found in his research that replacing 100% of recycled materials with natural materials reduces tensile capacity by about 15 to 20%. Furthermore, Fig. 12 also shows that the tensile

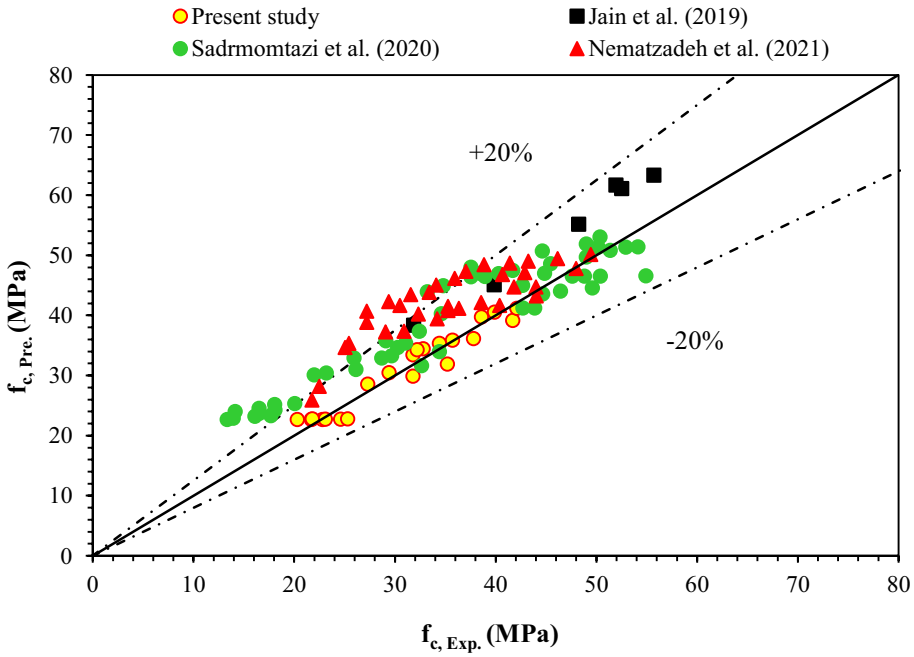

Fig.11 Comparison of the values of the developed model with the laboratory values reported in the literature and the present study

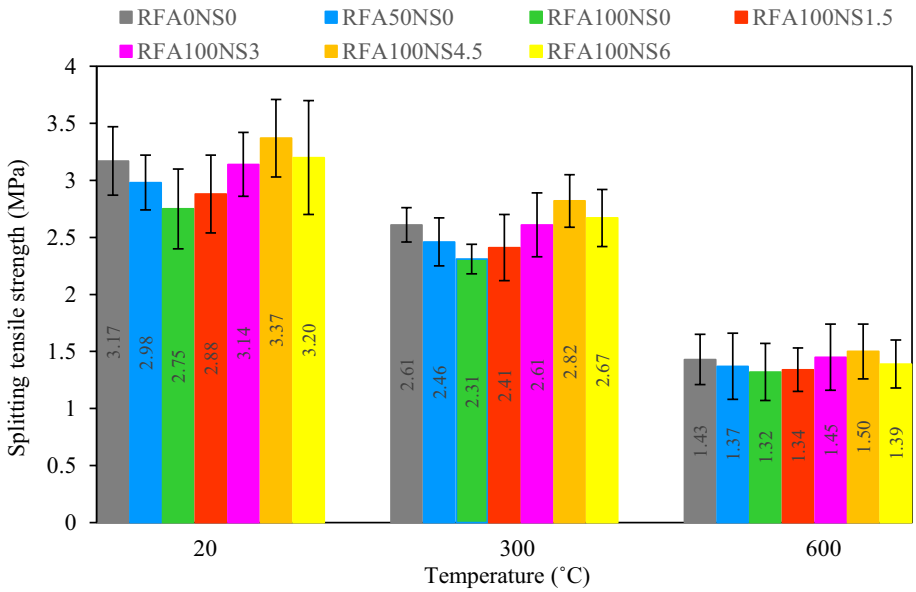

Fig.12 Splitting tensile capacity of concrete samples containing RFA and nano-silica per temperature

capacity of concretes containing RFA is increased by up to 6% when nano-silica is present. According to Table 4 and Fig. 12, in concrete containing RFA, the presence of 1.5 and 4.5% nano-silica resulted in the lowest and highest increases of 4.7 and 22.5%, respectively, in the tensile strength of concrete relative to the corresponding concrete lacking pozzolan. The increase in tensile strength is a result of an enhanced hydrated cement paste-aggregates bonding [44, 58]. As reported by Pacheco-Torgal, et al. [64], adding nano-silica as a weight substitute for cement in concrete makes ITZ more compact and stronger than conventional concrete. On the other hand, the use of more than 4.5% nano-silica in the samples with RFA reduces the improvement of tensile capacity at ambient temperature. This significant reduction appears to result from a high water uptake of recycled fine aggregate and nano-silica and the appearance of unstable lumps during hydration reaction in concrete.

Increasing the exposure temperature to 300 °C lowered the tensile capacity of all concrete samples. At this temperature according to Table 4, the tensile capacity of samples containing 0, 50, and 100% RFA reached 2.61, 2.46 and 2.31 MPa, showing a decrease of 17.7, 17.4 and 16%, respectively, in comparison to corresponding unheated samples. This trend shows that at this temperature, the amount of tensile capacity loss due to heat in concrete samples containing RFA is less than the loss of capacity of the reference sample (without RFA and nano-silica). Also, drops occurring in the tensile capacity of samples RFA100NS1.5, RFA100NS3, RFA100NS4.5 and RFA100NS6 at 300 °C compared to the similar unheated samples were from 16 to 17%. This decline is mainly due to chemical water evaporation initiation in cement paste and also internal cracks caused by temperature gradients [22]. Dried mortar stuck to the RFA particles and the presence of fine cracks in them allow the gases trapped in the pores to be released, which reduces the growth of cracks in the volume of concrete and thus reduces the harmful effects of cavitation. With increasing temperature to 600 °C, the decrease in tensile capacity of the heated concrete samples compared to the reference unheated samples varied from 52 to 57%, the lowest and highest of which are related to RFA100NS0 and RFA100NS6, respectively. This significant decrease is due to the formation of porosity induced by cement paste dehydration as well as the thermal incompatibility of components of concrete and the resulting gathering of internal stresses [22, 65]. On the other hand, nano-silica in concrete mix lowers the structural porosity of concrete and prevents the release of water vapor pressure due to heat, thus increasing the internal stresses in the concrete, which reduces the bearing capacity.

Normalized tensile capacity is the post-heating tensile capacity, f_{tT}, divided by the unheated tensile capacity, f_t, which is shown per temperature for test samples in Fig. 13. Further, Fig. 13 demonstrates normalized tensile capacity in terms of temperature according to EN 1992-1-2 [66], in which it is observed that the estimations of this standard are lower than the laboratory results of the normalized tensile capacity of the reference sample and the samples containing recycled fine nanoparticles and nano-silica at temperatures of 300 and 600 °C.

Using nonlinear regression, normalized tensile capacity ($\frac{f_{t(RF,NS,T)}}{f_{t(0,0,20)}}$ or $\frac{f_{tf}}{f_t}$) was presented in terms of temperature, the level of RFA replacement, and the percentage of nano-silica replacement for all concrete samples as Eq. (3), which has an appropriate coefficient of determination ($R^2 = 0.96$). Furthermore, the response level for the model

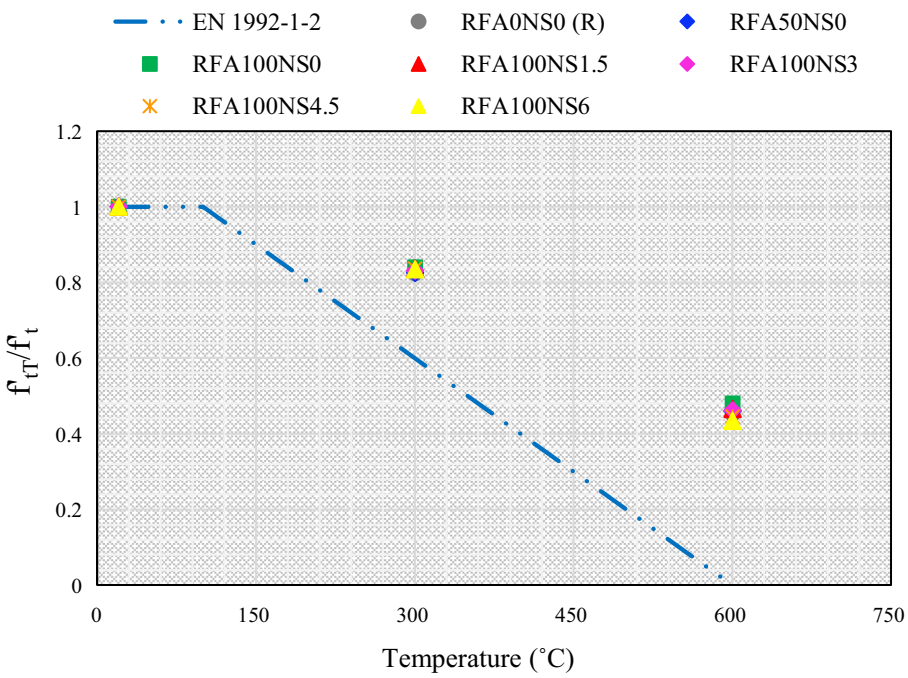

Fig.13 Normalized splitting tensile capacity in terms of temperature

obtained from Eq. (3) is presented in Fig. 14. According to Fig. 14, it can be seen that the normalized tensile capacity of concrete exposed to different temperatures increases with decreasing V_{RF} values (volume percentage of RFA) and increasing W_{NS} values (percentage of nano-silica powder replacement):

$$\frac{f_{tT}}{f_t} = \frac{f_{t(RF,NS,T)}}{f_{t(0,0,20)}} = \frac{1 - 0.13\ V_{RF}^{0.9} + 0.65\ W_{NS}^{0.47}}{1 + 3.86\ T'^{2.25}}$$
$$T' = \frac{T - 20}{1000} \qquad 0\% \le V_{RF} \le 100\%, \qquad 0\% \le W_{NS} \le 6\%. \tag{3}$$

To better understand the proposed model for tensile capacity and its verification, the model prediction results are compared with the laboratory results of this study and the results of other researchers (Fallah and Nematzadeh [44], Duarte, et al. [67], Wang, et al. [68], Agarwal, et al. [50], Gao, et al. [51] and Yonggui, et al. [53]) in Fig. 15. The proposed model can reliably estimate the empirical tensile strength data of samples with recycled aggregate and nano-silica in the unheated and heated cases.

Table 5 presents the equations of splitting tensile capacity in terms of compressive capacity by ACI 318-14 [69], EHE [70] and ACI 363-92 [71], CEB [72], GB 10010 [73] And NBR 6118 [74]. In addition, Fig. 16 compares these formulas with the test findings of this study. According to this figure, most codes predict the splitting tensile capacity of heated and unheated concrete samples with an overestimation, except for CEB and GB 10010, which provide acceptable estimates. On the other hand, EHE gives lower estimates for the tensile capacity results of samples. However, in this study, based on the considered variables, a correction factor is needed for providing a proper relationship between compressive capacity and splitting tensile capacity. Therefore, nonlinear regression was used to present Eq. (4) for heated samples incorporating recycled aggregates and nano-silica in terms of temperature. Based on Eq. (4), samples have a coefficient of determination of 0.94, indicating that the compressive capacity and splitting tensile capacity of samples containing RFA and nano-silica exposed to high temperatures correlate well. This good correlation can be due to the similar behaviors of the samples in the splitting tensile capacity test and the compressive capacity test:

$$f_t = \alpha f_c^{0.5}$$
$$\alpha = \frac{(1 + 0.0037\ V_{RF})(0.98e^{-0.03\ T'}) + 0.071\ W_{NS}}{(1 - 1.2\ W_{NS} + e^{1.45\ T'})} R^2 = 0.94$$
$$T' = \left(\frac{T - 20}{1000}\right). \tag{4}$$

4.4 Modulus of elasticity

The post-heating moduli of elasticity of samples containing RFA and nano-silica are shown in Fig. 17. By replacing recycled materials with natural materials, the modulus of elasticity values dropped. In the unheated case, with

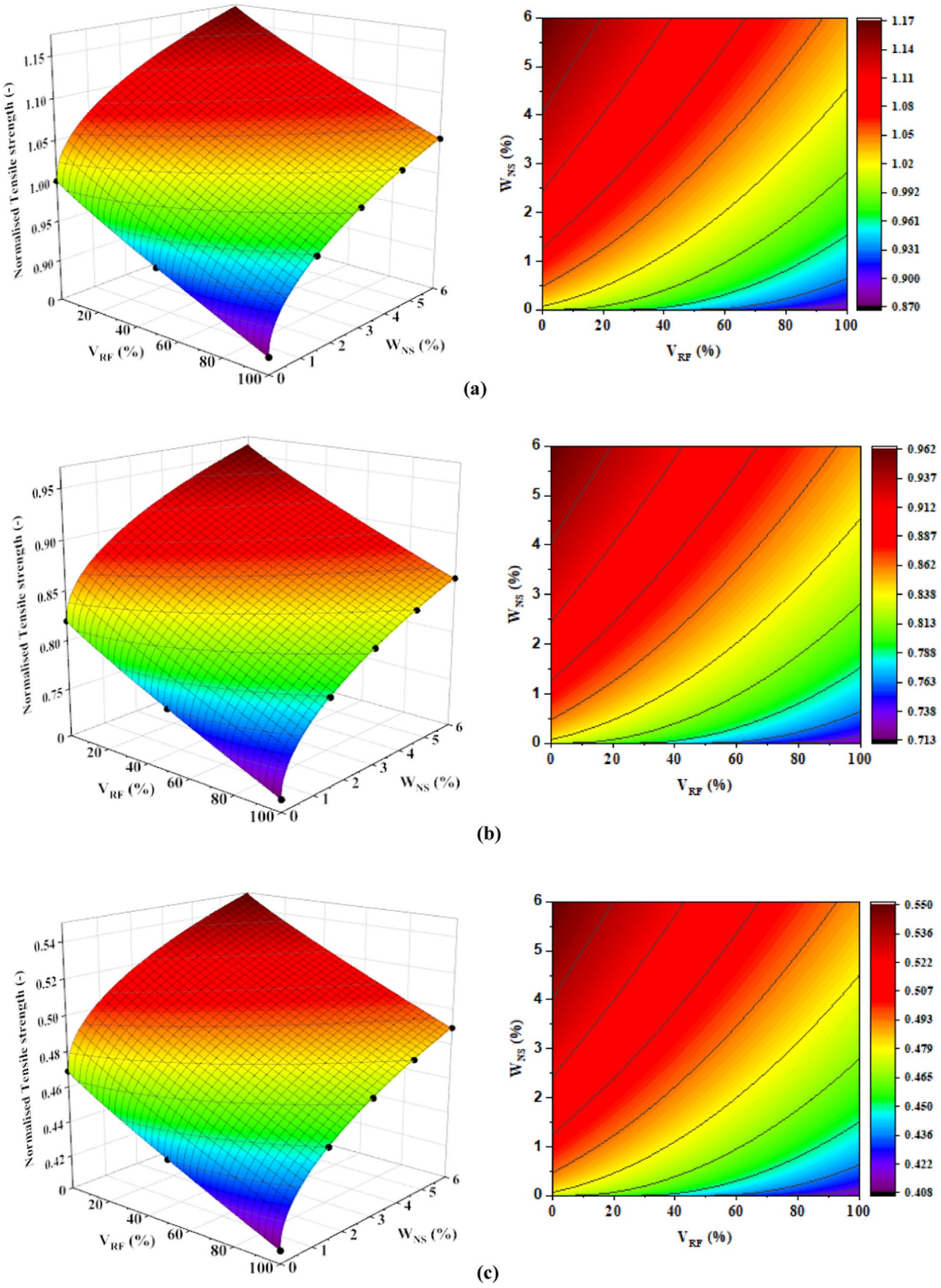

Fig.14 Response level of the proposed splitting tensile strength model at different temperatures **a** 20 °C, **b** 300 °C and **c** 600 °C

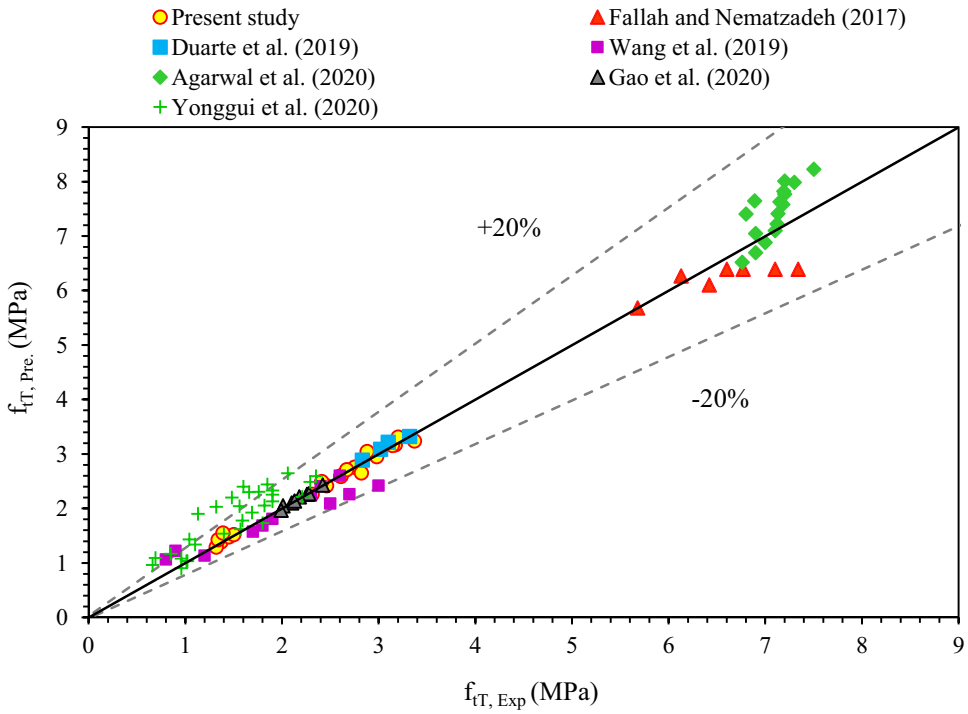

Fig.15 Predictive results of the proposed equation of tensile strength versus laboratory results of the present study and other research

Table 5 Splitting tensile capacity equation provided by various codes

Code	Relationship
ACI 318–14 [69]	$f_t = 0.56\sqrt{f_c}$
EHE [70]	$f_t = 0.21 f_c^{\frac{2}{3}}$
ACI 363–92 [71]	$f_t = 0.59\sqrt{f_c}$
CEB [72]	$f_t = 1.56(\frac{f_c-8}{10})^{\frac{2}{3}}$
GB 10010 [73]	$f_t = 0.19 f_c^{0.75}$
NBR 6118 [74]	$f_t = 0.3 f_c^{(\frac{2}{3})}$

f_c Concrete compressive capacity (MPa), f_t splitting tensile capacity (MPa)

an increase in the volume of RFA by 50 and 100% compared to the reference sample, the modulus of elasticity dropped by 13.2 and 23.5%, respectively. The reason for the modulus reduction of samples containing RFA compared to samples without recycled aggregates is the poor physical structure of these recycled materials, which have less resistance to deformation compared to natural sand. Therefore, the modulus values of concrete components affect the modulus of elasticity of concrete. Furthermore, according to Fig. 17, incorporating nano-silica into RFA concrete leads to a higher modulus of elasticity. Incorporating nano-silica reduces the porosity and increases the bond level of cement paste with aggregate and in turn, increases the concrete hardness; thus, an increase in modulus of elasticity results from an increased concrete hardness from adding fine pozzolanic Nano-silica particles. For concrete containing RFA, incorporating 1.5 and 6% nano-silica resulted in the lowest and highest modulus increases of 4 and 18%, respectively, relative to the corresponding concrete lacking pozzolan. With increasing temperature to 300 °C, the modulus values decreased significantly, such that samples RFA0NS0, RFA50NS0, and RFA100NS0 saw modulus drops of 30.6, 24.8, and 22.5% compared to the modulus values in the unheated case. The observed drops may result from free water and chemical C-S-H water escaping, which causes microcracks in the concrete and ultimately leads to a reduction in hardness. Also, at this temperature, according to the figure, modulus values of samples RFA100NS1.5, RFA100NS3, RFA100NS4.5, and RFA100NS6 decreased by 21.1, 22.2, 23.1, and 26.5%, respectively, relative to that of the similar unheated sample. Furthermore, Fig. 17 indicates that at 300 °C, the addition of nano-silica as a weight substitute for cement to concrete containing RFA increased the concrete modulus by 17%. For 600 °C, a higher drop rate was seen in the modulus of elasticity than that for 300 °C. At this temperature, in the presence of 0, 50, and 100% RFA replacement, the modulus experienced a decrease of 71.4, 69, and 67.8%, respectively, in comparison with the similar unheated sample. Furthermore, modulus values of RFA concrete drooped by 67.7, 70, 71.2 and 72.6% by incorporating 1.5, 3, 4.5, and 6% nano-silica, respectively, relative to the similar unheated sample. At 600 °C, a higher rate of dehydration of calcium hydroxide leads to a notable C-S–H gel decomposition, giving rise to greater cement

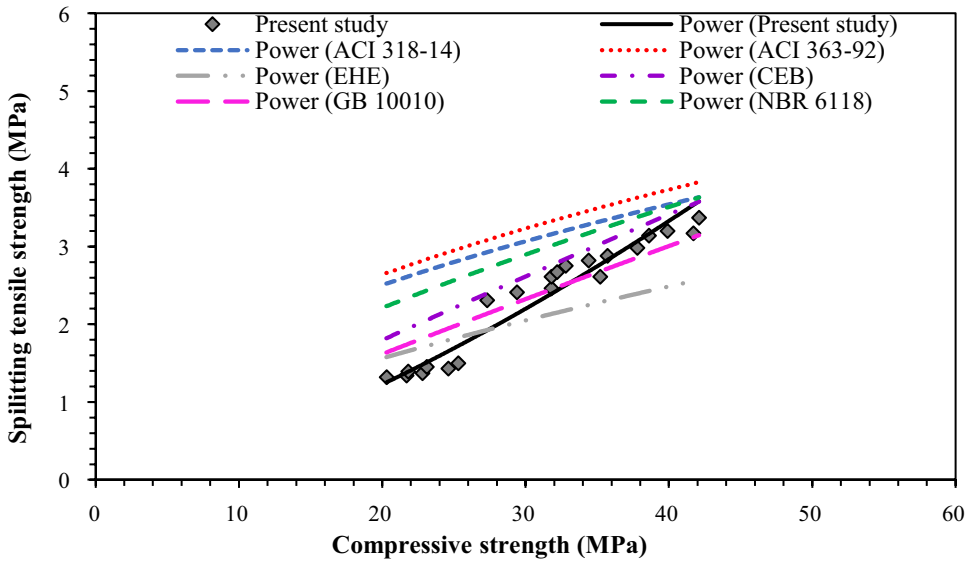

Fig. 16 Results of codes in comparison with those of test samples

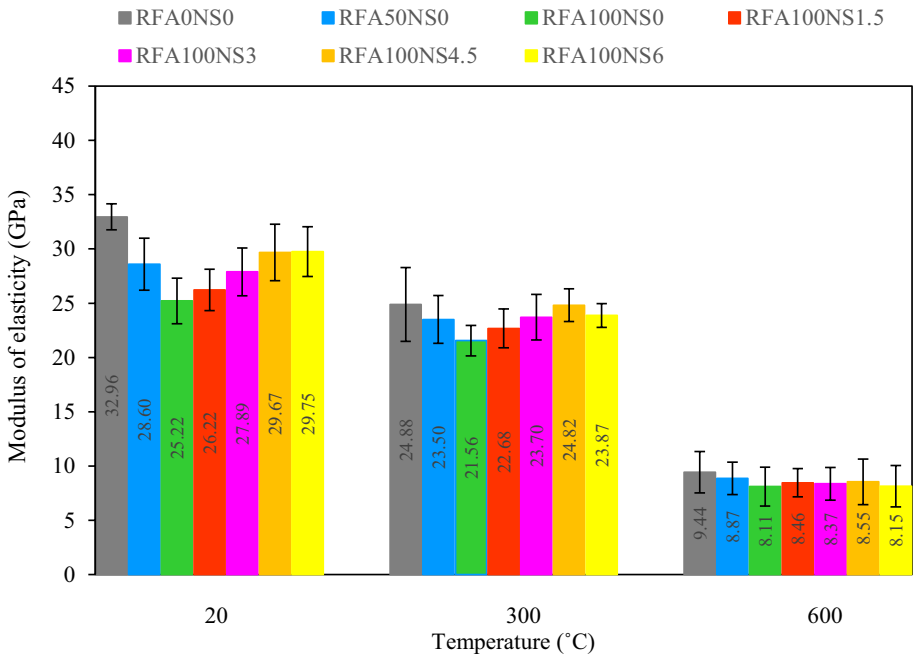

Fig.17 Modulus of elasticity of samples containing RFA and nano-silica after exposure to heat

paste porosity, more ITZ microcracks, and thus increased axial deformation. For 600 °C, the minimum and maximum values of modulus of elasticity are 8.1 and 9.4 GPa, respectively, for RFA100NS0 and RFA0NS0.

The normalized modulus of elasticity is the modulus value of a heated concrete sample divided by that of a similar unheated sample. The normalized modulus of elasticity results for all groups is shown in Fig. 18. In addition, Fig. 18 gives the normalized modulus of elasticity predictions of ACI 216 [47] and EN 1994-1-2 [49] for heated samples. It shows that the laboratory normalized modulus results of all heated samples are underestimated by EN 1994-1-2 [49], while these results are underestimated by ACI 216 [47] up to 300 °C and are well estimated for concrete samples after exposure to 600 °C.

The relationship for normalized modulus $\frac{E_{c(RF,NS,T)}}{E_{c(0,0,20)}}$ (or $\frac{E_{cT}}{E_c}$) was determined as Eq. (5) by using nonlinear regression analysis in terms of RFA volume percentage, nano-silica weight percentage, and temperature for all concrete samples. This equation has a very high coefficient of determination ($R^2 = 0.99$):

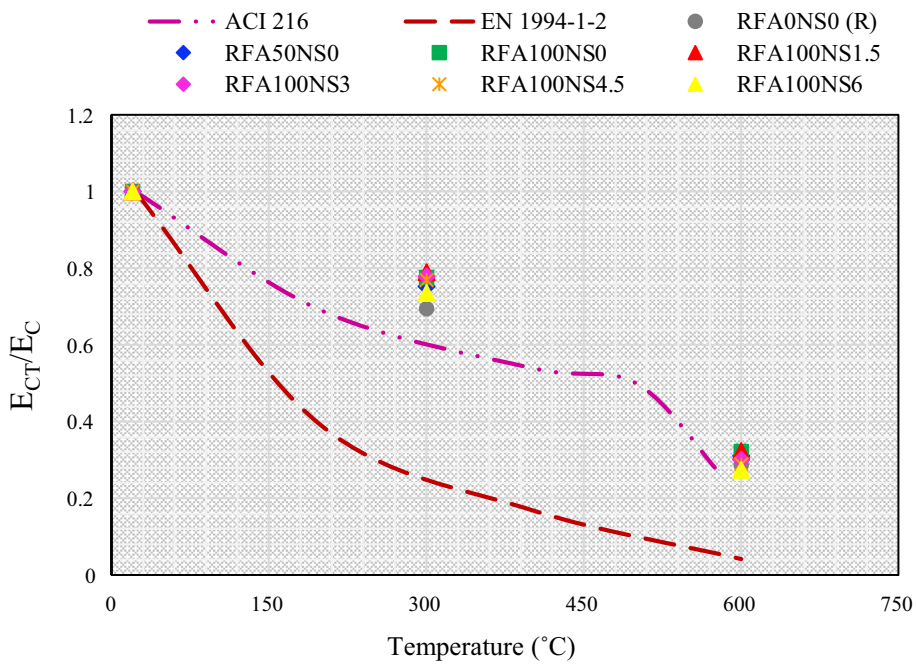

Fig.18 Normalized modulus of elasticity of samples per temperature

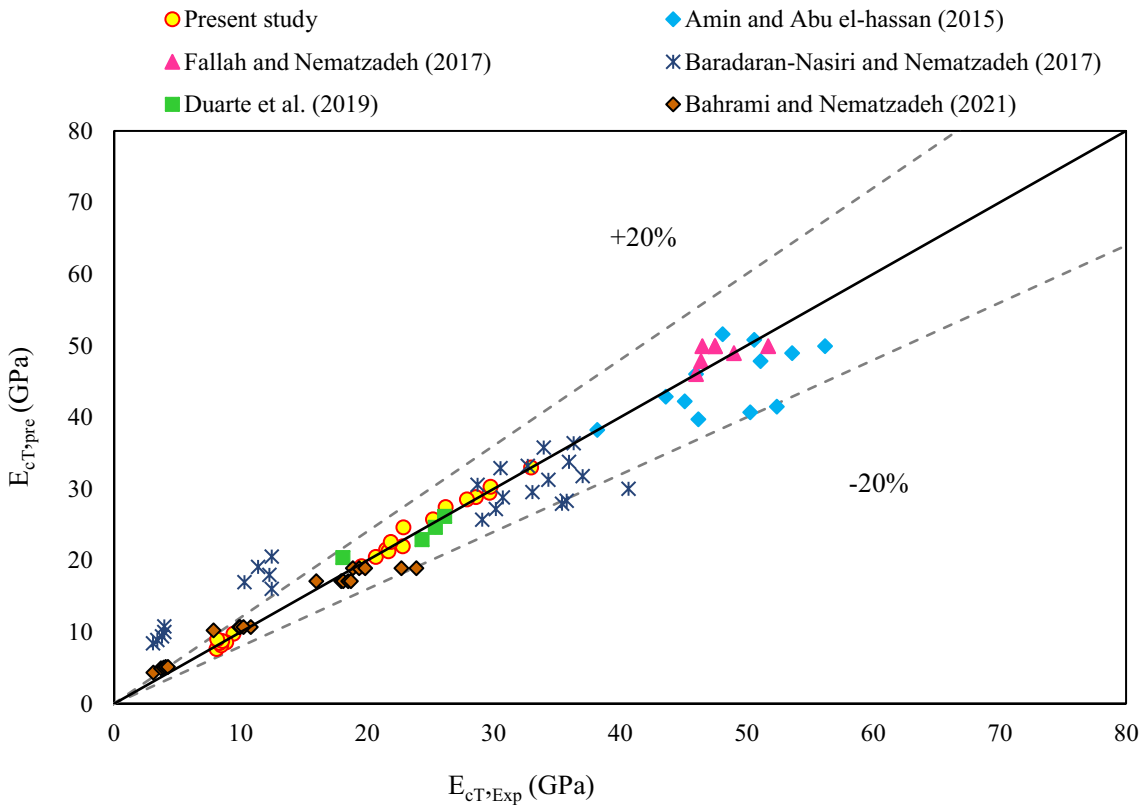

Fig.19 Comparison of the results of the presented modulus of elasticity model with the laboratory data of other researchers

$$\frac{E_{cT}}{E_c} = \frac{E_{c(RF,NS,T)}}{E_{c(0,0,20)}} = \frac{1 - 0.22\ V_{RF}^{0.81} + 0.99\ W_{NS}^{0.7}}{1 + 10.2\ T'^{2.67}}$$
$$0\% \le V_{RF} \le 100\%,\ 0\% \le W_{NS} \le 6\% T' = \frac{T - 20}{1000}. \quad (5)$$

Figure 19 compares the results of the elastic modulus prediction with the laboratory results of other researchers (Amin and Abu el-Hassan [19], Fallah and Nematzadeh [44], Baradaran-Nasiri and Nematzadeh [27], Duarte, et al. [67] and Bahrami and Nematzadeh [23]). From Fig. 19, it can be concluded that the presented model for the modulus of elasticity agrees well with empirical findings reported by other researchers.

Also, the relationship presented as $E_c = 4700\sqrt{f_c}$ in ACI 318 [69] gives the compressive capacity in terms of the modulus of elasticity. However, in this study, based on the considered variables, a correction factor is needed for obtaining a proper equation for compressive capacity and modulus of elasticity. Nonlinear regression was used to provide Eq. (6) to express the modulus of elasticity and compressive capacity of concrete samples based on variables considered in the tests:

$$E_c = \alpha f_c^{0.5}\ \alpha = \frac{(6700 - 182 V_{RF})(1.524 e^{8.74T'}) + 6140 W_{NS}}{(1 + 5 W_{NS} + e^{11.7T'})}$$
$$R^2 = 0.95\ T' = \left(\frac{T - 20}{1000}\right). \quad (6)$$

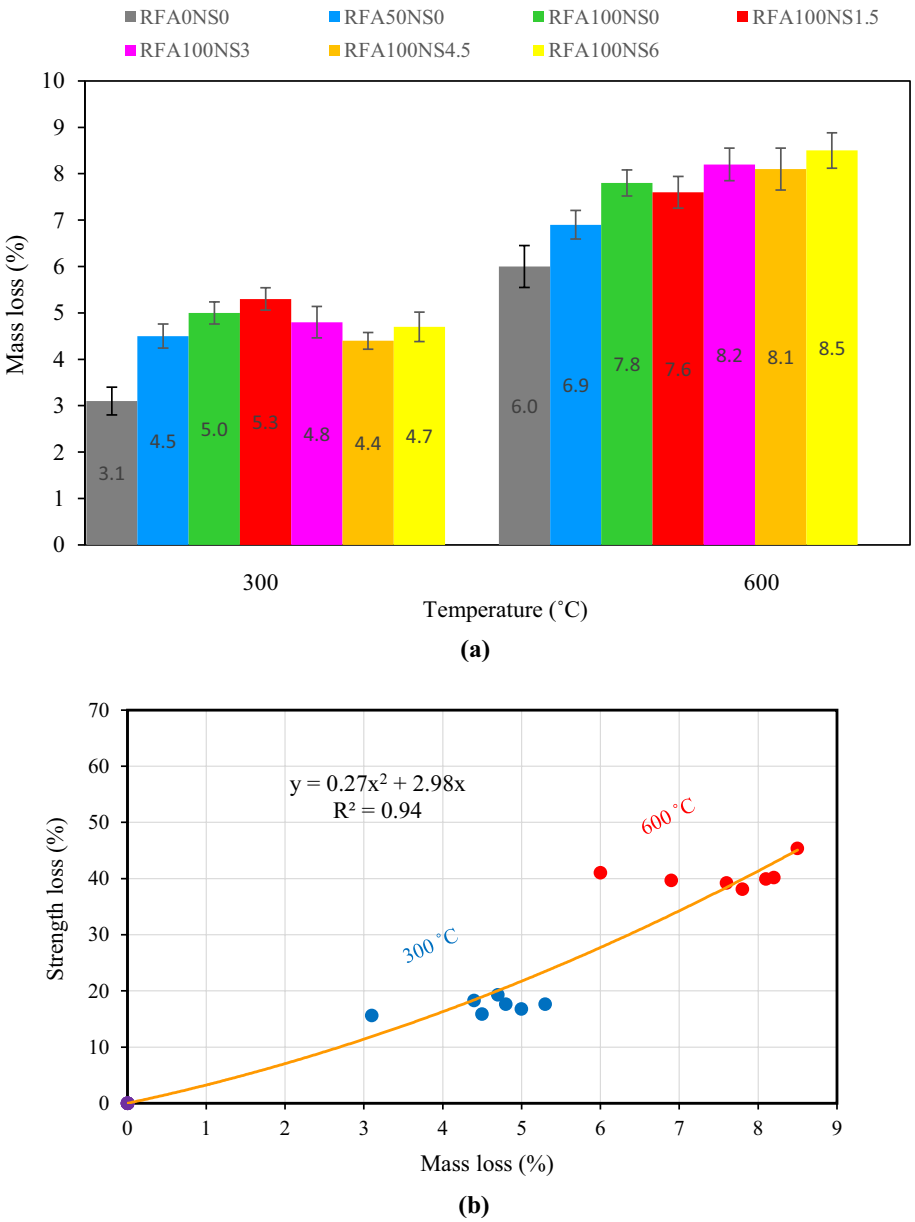

Fig.20 Weight loss of concrete samples; **a** Percentage of weight loss with temperature, **b** The relationship between weight loss and capacity loss exposed to high temperature

4.5 Mass loss after exposure to heat

The pre- and post-heating weights of the samples were determined to find out how much weight each sample group had lost. The weight loss rate of the samples after experiencing different elevated temperatures was compared to that of corresponding unheated samples in Fig. 20. Figure 20a shows that the weight loss of the samples increased with the temperature, predominantly as a result of the evaporation of concrete physical and surface water, dehydration and increased decomposition rate of hydrated products of the cement paste with increasing heat. The physicochemical alterations of concrete after exposure to 300 °C result from the release of free water and chemically bound water in the C-S-H gel [22]. After 600 °C, a greater loss occurred in the weight of the concrete, which is attributed to the onset of the degradation of C-S-H gel and $Ca(OH)_2$ (Portlandite) and the evaporation of chemical water in them [55, 75]. Also, using RFA in concrete in place of natural fine aggregate increased the post-fire loss of weight of the samples; thus, the sample containing 100% RFA showed a greater weight loss than the sample containing 50% RFA. With a rise in the quantity of recycled fine particles in mixing design, the pores of the samples increased, and with exposure to heat, more water vapor escaped from the sample, which led to more weight loss. In addition, a lower rate of increase in weight loss of the concrete samples with increasing nano-silica replacement percentage relative to the sample lacking nano-silica (RFA100NS0) was observed. The highest weight loss occurred in RFA100NS6 concrete sample at 600 °C with a drop of 8.5% compared to the corresponding unheated sample, while the reference sample (RFA0NS0) with 6% loss had the lowest weight loss among other samples. Nano-silica pozzolan substituting for cement forms C-S-H gel through pozzolanic reactions with $Ca(OH)_2$ due to cement hydration. At high temperatures, this CSH gel begins to decompose and as a result, empty space is created in concrete, which reduces the sample weight [76]. Figure 20b demonstrates the variation of weight loss with capacity for the heated samples. The figure indicates that the weight loss and the capacity drop for concrete containing RFA and nano-silica are directly related to each other after exposure to high temperatures. Regression analysis was used on the empirical results of these two parameters, to determine Eq. (7) with a very appropriate coefficient of determination ($R^2 = 0.94$). This relationship shows that the percentage of capacity loss of different samples is about 3.5 to 7 times the percentage of weight loss:

$$y = 0.27\,x^2 + 2.98\,x. \tag{7}$$

In the above, x and y are losses in the weight and capacity of heated samples in percentage, respectively.

4.6 Scanning electron microscopy (SEM)

Scanning electron microscopy (SEM) images are a convenient tool for testing and analyzing concrete microstructures at the micrometer scale. Figure 21 shows the SEM images of RFA0NS0, RFA100NS0 and RFA100NS4.5. Figure 21a shows the ITZ of natural fine aggregates and the hydrated cement paste and indicates the proper bonding of the two materials. On the other hand, Fig. 21b shows defective bonding and incomplete recycled aggregates–hydrated cement cohesion. According to SEM results, old mortar adhering to recycled aggregates weakens ITZ relative to normal concrete (concrete lacking recycled aggregates) and creates microcracks and higher porosity in the hydrated cement matrix. As these two parts are not well connected, concrete capacity declines. Therefore, ordinary concrete has less porosity than concrete containing 100% RFA at ambient temperature. Also, Fig. 21c indicates that the sample containing 4.5% nano-silica (RFA100NS4.5) has less porosity than concrete without nano-silica (RFA100NS0). Although one could distinguish the old mortar and the new mortar considering their differing microstructure and pore structure, it seems that the two parts have developed a good bond given their very compact ITZ. The microstructural compactness of ITZ results from the effect of the addition of silica nanoparticles. These nanoparticles can result in dense ITZ via two mechanisms: a physical and a chemical mechanism. The first case can be due to higher specific surface area and finer dimensions of pozzolan relative to cement. The second comes from the chemical tendency of nano-silica to react with $Ca(OH)_2$ (a product of cement hydration), which improves the aggregate-hydrated cement matrix bond. This improved bond is reactive since calcium hydroxide is converted to CSH gel through silica. Therefore, it seems that these two mechanisms are the most important reasons for the higher capacity of recycled concrete containing nano-silica. Moreover, Fig. 21c demonstrates that the crystalline form of nano-silica particles is spherical, in which the uniform distribution of particles is evident.

In addition, Fig. 22 shows the post-heating SEM images of RFA0NS0 (reference concrete), RFA100NS0, and RFA100NS4.5 samples. It is seen that different chemical compounds can be detected in cement paste as well as microcracks and cavities. In these images, C-S-H gel can be seen as a foam nanostructure (solid gray masses). In addition, Fig. 22 shows ordinary concrete and recycled concrete cracking due to high heat. Cracking in concrete due to heat can be ascribed to water vapor pressure inside the cavities

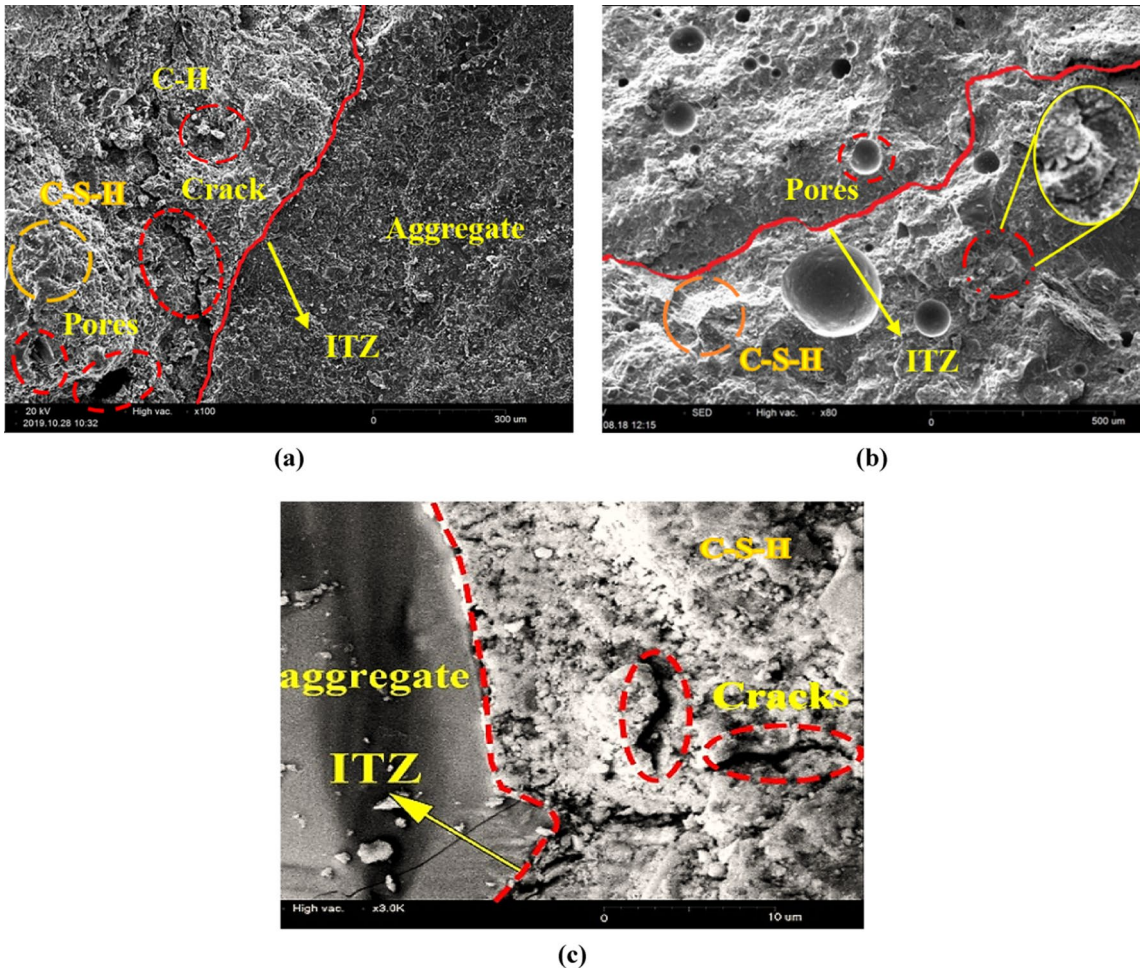

(a) (b) (c)

Fig.21 SEM images: **a** Concrete containing natural aggregates without pozzolan (RFA0NS0); **b** concrete containing recycled aggregates without nano-silica (RFA100NS0); and **c** concrete containing recycled aggregates and 4.5% nano-silica (RFA100NS4.5)

of concrete; this gives rise to the spalling phenomenon [35]. Nevertheless, cavities observed on the fracture surface of the concrete after exposure to 600 °C may be a result of the evaporation and chemical decomposition of water in calcium hydroxide crystals and the considerable C-S-H gel decomposition. This leads to more cavities in the cement paste and the formation of microcracks in ITZ, in turn leading to surface microcracks and internal stresses. After the release of free water and chemical water of the samples at high temperatures, the C-S-H nanostructure became larger and the size of this spongy structure increased.

According to studies, calcium hydroxide crystals (Portlandite) begin to decompose and turn into limestone (hydroxylation process) between temperatures of 400–600 °C [22]. Calcium carbonate also decomposes at 600 °C and turns into lime. Finally, according to Fig. 22a–c, C-S-H decomposes almost completely at 600 °C, causing cracks and cavities. Furthermore, the figures show that the porosity of the concretes increases with increasing temperature.

5 Conclusions

The residual features of concretes incorporating RFA replacing natural sand and nano-silica pozzolan replacing cement before and after exposure to the fire were addressed. Different parameters comprising the compressive capacity, splitting tensile capacity, ultrasonic pulse velocity (UPV), elastic modulus, and weight drop of the samples were evaluated. Moreover, empirical findings for the mechanical features of the heated concrete were assessed against predictions of ACI 216, EN 1994-1-2, EN 1992-1-2, and ASCE. Ultimately, it was attempted to predict the post-fire mechanical features of concrete with RFA and nano-silica by developing empirical equations. The main results obtained in this study are provided below:

1. The presence of nano-silica and a rise in its quantity in RFA concrete improved the load-bearing capacity compared with the control sample (by 9–28%) for all the exposure temperatures, such that the replacement per-

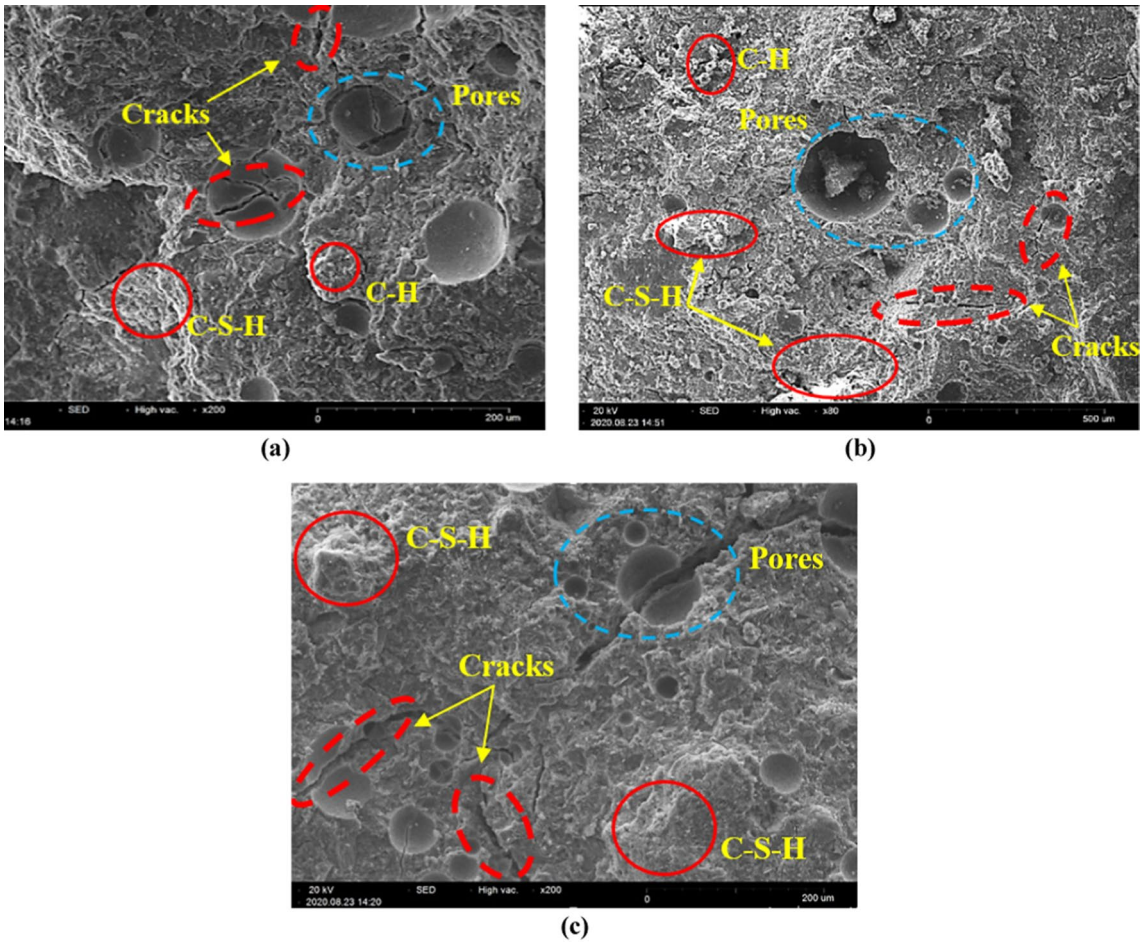

Fig.22 SEM images of samples after 600 °C: **a** RFA0NS0, **b** RFA100NS0 and **c** RFA100NS4.5

centage of 4.5% resulted in the maximum improvement. Moreover, a rise in the exposure temperature lowered the strength of the recycled samples, and this reduction was more pronounced at higher replacement levels.

2. The UPVs of samples in the unheated and heated cases saw a decline when the replacement quantity of the RFA increased, with a more significant decline in the unheated samples. On the other hand, the UPVs of the heated and unheated samples increased with a rise in the quantity of nano-silica in concrete containing RFA, whereas using more than 4.5% nano-silica led to a drop in UPV. By raising the temperature, a significant decline was seen in the UPVs of the concretes; this drop was more significant in the recycled samples containing nano-silica compared with the sample without nano-silica.
3. The incorporation of RFA reduced the splitting tensile capacity of the unheated and heated samples (by 8–13%). As the nano-silica content of the recycled samples increased by up to 6%, the tensile capacity improved, such that the maximum improvement occurred in the recycled sample containing 4.5% nano-silica. After 600 °C, the highest drop of 57% occurred in the tensile capacity of concrete relative to the unheated case in the recycled sample containing the highest nano-silica replacement percentage.
4. Replacing the natural sand with the RFA decreased the elastic moduli of the heated and unheated samples, with a smaller drop in the heated concrete samples. In addition, with a rise in nano-silica quantity, the elastic moduli of the heated and unheated concrete increased by 5–18%. With a rise in temperature, a notable drop occurred in the elastic modulus of all the samples relative to the unheated case (by 68–73% post-exposure to 600 °C), and the maximum value of this decline occurred in the recycled concrete with the highest nano-silica content.
5. Raising the exposure temperature increased the heat-induced loss of weight in samples (by 6–8.5%). The incorporation of RFA and nano-silica in the concretes increased the weight loss in the heated samples (at

600 °C), with the greatest weight loss in the recycled sample containing the highest replacement percentage of nano-silica and recycled aggregate.

6. Codes ACI 216, ASCE, and EN 1994-1-2 properly estimated the empirical findings of the normalized post-fire capacity of the samples. Furthermore, the predictions of ACI 216 regarding the normalized elastic modulus of the heated concretes were close to the experimental results to a large extent, contrary to the case with EN 1994-1-2, while an underestimation was observed for the predictions of EN 1994-1-2. In addition, the EN 1992-1-2 code provided a significant underestimation of the normalized tensile capacity of the concrete samples at all temperatures.
7. A general formula between the compressive strength and UPV was developed as a polynomial for all the hated concrete samples containing different volume contents of RFA and nano-silica that showed proper correlation with the experimental results. Additionally, equations with proper accuracy were presented to predict compression capacity, splitting tensile capacity, and elastic modulus of the samples after exposure to fire considering the parameters of temperature and replacement percentage of RFA and nano-silica; these equations demonstrated proper correlation with the empirical findings of the present work and others.
8. The fracture surface in the concrete without the RFA was regular and smooth, in which cracking passed through the aggregate particles. However, with a rise in the RFA quantity, a tortuous and irregular surface was observed. After experiencing 600 °C, pores appeared at the fracture surface, such that the coarse particles could easily be removed by hand. In addition, with a rise in the temperature, fewer microcracks formed in the samples containing only the recycled aggregate compared with those containing both RFA and nano-silica, while the recycled samples containing nano-silica showed the most microcracks.

Funding This study was not supported by foundation.

Data availability The datasets generated during and/or analyzed during the current study are available from the corresponding author on reasonable request.

Declarations

Conflict of interest The authors declare that there is no conflict of interest in this work.

Ethical approval This article does not contain any studies with human participants or animals performed by any of the authors.

References

1. Roziere E, Bendimerad AZ, Samouh H, Loukili A. Assessing the relaxation of recycled aggregates concrete from free and restrained shrinkage tests. J Build Eng. 2023;64: 105549.
2. Datta SD, Sobuz MHR, Akid ASM, Islam S. Influence of coarse aggregate size and content on the properties of recycled aggregate concrete using non-destructive testing methods. J Build Eng. 2022;61: 105249.
3. Velay-Lizancos M, Martinez-Lage I, Vazquez-Burgo P. The effect of recycled aggregates on the accuracy of the maturity method on vibrated and self-compacting concretes, archives of civil and mechanical. Engineering. 2019;19:311–21.
4. Rezaei F, Memarzadeh A, Davoodi M-R, Dashab M-A, Nematzadeh M. Mechanical features and durability of concrete incorporating recycled coarse aggregate and nano-silica: experimental study, prediction, and optimization. J Build Eng. 2023;73: 106715.
5. Santos SA, da Silva PR, De Brito J. Durability evaluation of self-compacting concrete with recycled aggregates from the precast industry. Mag Concr Res. 2019;71(24):1265–82.
6. Solyman M, Classification of recycled sands and their applications as fine aggregates for concrete and bituminous mixtures, 2005.
7. Evangelista L, De Brito J. Concrete with fine recycled aggregates: a review. Eur J Environ Civ Eng. 2014;18(2):129–72.
8. Nam J, Kim G, Yoo J, Choe G, Kim H, Choi H, Kim Y. Effectiveness of fiber reinforcement on the mechanical properties and shrinkage cracking of recycled fine aggregate concrete. Materials. 2016;9(3):131.
9. Akono A-T, Zhan M, Chen J, Shah SP. Nanostructure of calcium-silicate-hydrates in fine recycled aggregate concrete. Cement Concr Compos. 2021;115: 103827.
10. Pedro D, De Brito J, Evangelista L. Structural concrete with simultaneous incorporation of fine and coarse recycled concrete aggregates: mechanical, durability and long-term properties. Constr Build Mater. 2017;154:294–309.
11. Cantero B, Sáez del Bosque IF, Matías A, Sánchez de Rojas MI, Medina C. Inclusion of construction and demolition waste as a coarse aggregate and a cement addition in structural concrete design, archives of civil and mechanical. Engineering. 2019;19:1338–52.
12. Rodrigues P, Silvestre JD, Flores-Colen I, Viegas CA, Ahmed HH, Kurda R, de Brito J. Evaluation of the ecotoxicological potential of fly ash and recycled concrete aggregates use in concrete. Appl Sci. 2020;10(1):351.
13. Gao D, Wang F. Effects of recycled fine aggregate and steel fiber on compressive and splitting tensile properties of concrete. J Build Eng. 2021;44: 102631.
14. Fallah-Valukolaee S, Nematzadeh M. Experimental study for determining applicable models of compressive stress–strain behavior of hybrid synthetic fiber-reinforced high-strength concrete. Eur J Environ Civ Eng. 2020;24(1):34–59.
15. Chen X-F, Jiao C-J. Microstructure and physical properties of concrete containing recycled aggregates pre-treated by a nano-silica soaking method. J Build Eng. 2022;51: 104363.
16. Jagadisha A, Rao KB, Nayak G, Kamath M. Influence of nano-silica on the microstructural and mechanical properties of high-performance concrete of containing EAF aggregate and processed quarry dust. Constr Build Mater. 2021;304: 124392.
17. Li H, Xiao H-G, Yuan J, Ou J. Microstructure of cement mortar with nano-particles. Compos B Eng. 2004;35(2):185–9.
18. Fallah-Valukolaee S, Mousavi R, Arjomandi A, Nematzadeh M, Kazemi M. A comparative study of mechanical properties and

life cycle assessment of high-strength concrete containing silica fume and nanosilica as a partial cement replacement. Structures: Elsevier; 2022. p. 838–51.
19. Amin M, Abu el-Hassan K. Effect of using different types of nano materials on mechanical properties of high strength concrete. Constr Build Mater. 2015;80:116–24.
20. Palla R, Karade S, Mishra G, Sharma U, Singh L. High strength sustainable concrete using silica nanoparticles. Constr Build Mater. 2017;138:285–95.
21. Sravanti C, Sreeparvathy C. Influence of nano silica on mechanical strength of ground nut shell ash concrete. Mater Today Proc. 2022;51:455–9.
22. Hertz KD. Concrete strength for fire safety design. Mag Concr Res. 2005;57(8):445–53.
23. Bahrami A, Nematzadeh M. Effect of rock wool waste on compressive behavior of pumice lightweight aggregate concrete after elevated temperature exposure. Fire Technol. 2021;57(3):1425–56.
24. Da Silva JB, Pepe M, Toledo Filho RD. High temperatures effect on mechanical and physical performance of normal and high strength recycled aggregate concrete. Fire Saf J. 2020;117:103222.
25. Tanyildizi H, Coskun A. Performance of lightweight concrete with silica fume after high temperature. Constr Build Mater. 2008;22(10):2124–9.
26. Liu Y, Wang W, Chen YF, Ji H. Residual stress-strain relationship for thermal insulation concrete with recycled aggregate after high temperature exposure. Constr Build Mater. 2016;129:37–47.
27. Baradaran-Nasiri A, Nematzadeh M. The effect of elevated temperatures on the mechanical properties of concrete with fine recycled refractory brick aggregate and aluminate cement. Constr Build Mater. 2017;147:865–75.
28. Bui NK, Satomi T, Takahashi H. Effect of mineral admixtures on properties of recycled aggregate concrete at high temperature. Constr Build Mater. 2018;184:361–73.
29. ASTM C33/C33M Standard Specification for Concrete Aggregates. United States: American Society for Testing and Materials International, 2018.
30. ACI Committee 211.1–9.1 Standard practice for selecting proportions for normal, heavyweight, and mass concrete. ACI manual of concrete practice, Part1, American Concrete Institute, Michigan (USA), American Concrete Institute Farmington Hills. 2000; pp.38.
31. Nematzadeh M, Maghferat A, Herozi MRZ. Mechanical properties and durability of compressed nylon aggregate concrete reinforced with forta-ferro fiber: experiments and optimization. J Build Eng. 2021;41: 102771.
32. Fallahnejad H, Davoodi MR, Nikbin IM. The influence of aging on the fracture characteristics of recycled aggregate concrete through three methods. Struct Concr. 2021;22:E74–93.
33. ASTM C143/C143M. Standard Test Method for Slump of Hydraulic-Cement Concrete. United States: American Society for Testing and Materials International. 2015.
34. ASTM C192/C192M. Standard Practice for Making and Curing Concrete Test Specimens in the Laboratory. Philadelphia: Annual book of ASTM Standards; 2018.
35. Nematzadeh M, Tayebi M, Samadvand H. Prediction of ultrasonic pulse velocity in steel fiber-reinforced concrete containing nylon granule and natural zeolite after exposure to elevated temperatures. Constr Build Mater. 2021;273: 121958.
36. Nematzadeh M, Karimi A, Fallah-Valukolaee S. Compressive performance of steel fiber-reinforced rubberized concrete core detached from heated CFST. Constr Build Mater. 2020;239: 117832.
37. Nematzadeh M, Memarzadeh A, Karimi A. Post-fire elastic modulus of rubberized fiber-reinforced concrete-filled steel tubular stub columns: experimental and theoretical study. J Constr Steel Res. 2020;175: 106310.
38. EN, B. Testing hardened concrete. Method of determination of compressive strength of concrete cubes. BS EN 12390 Part, 3. 2000.
39. ASTM C597. Standard test method for pulse velocity through concrete. United States: American Society for Testing and Materials International. 2016.
40. ASTM C597. Standard test method for splitting tensile strength of cylindrical concrete specimens. Philadelphia: Annual Book of ASTM Standards; 2017.
41. ASTM C597. Standard test method for static modulus of elasticity and Poisson's ratio of concrete in compression. Philadelphia: Annual book of ASTM standards; 2014.
42. International Organization for Standardization. Fire-resistance Tests: Elements of Building Construction. Commentary on Test Method and Guide to the Application of the Outputs from the Fire-resistance Test. ISO834, 2012.
43. Kurda R, de Brito J, Silvestre JD. Water absorption and electrical resistivity of concrete with recycled concrete aggregates and fly ash. Cement Concr Compos. 2019;95:169–82.
44. Fallah S, Nematzadeh M. Mechanical properties and durability of high-strength concrete containing macro-polymeric and polypropylene fibers with nano-silica and silica fume. Constr Build Mater. 2017;132:170–87.
45. Nematzadeh M, Mousavi R. Post-fire flexural behavior of functionally graded fiber-reinforced concrete containing rubber. Comput Concr. 2021;27(5):417–35.
46. Dabbaghi F, Dehestani M, Yousefpour H, Rasekh H, Navaratnam S. Residual compressive stress–strain relationship of lightweight aggregate concrete after exposure to elevated temperatures. Constr Build Mater. 2021;298: 123890.
47. ACI (American Concrete Institute). Guide for determining the fire endurance of concrete elements. ACI 216R-89, Farmington Hills, 1989.
48. ASCE. Structural Fire Protection, ASCE Committee on Fire Protection. In: Structural Division. New York: American Society of Civil Engineers; 1992.
49. Eurocode 4. EN 1994–1–2. Design of composite steel and concrete structures–Part 1–2: General rules for structural fire design, 2004.
50. Agarwal A, Bhusnur S, Priya TS. Experimental investigation on recycled aggregate with laboratory concrete waste and nano-silica. Mater Today Proc. 2020;22:1433–42.
51. Gao C, Huang L, Yan L, Jin R, Chen H. Mechanical properties of recycled aggregate concrete modified by nano-particles. Constr Build Mater. 2020;241: 118030.
52. Alhawat M, Ashour A. Bond strength between corroded steel and recycled aggregate concrete incorporating nano silica. Constr Build Mater. 2020;237: 117441.
53. Yonggui W, Shuaipeng L, Hughes P, Yuhui F. Mechanical properties and microstructure of basalt fibre and nano-silica reinforced recycled concrete after exposure to elevated temperatures. Constr Build Mater. 2020;247: 118561.
54. IS 13311–1 (1992) Method of Non-destructive Testing of Concrete. Part 1: Ultrasonic Pulse Velocity Bureau of Indian Standard, New Delhi
55. Hossain-Zada MK, Kolagar S, Fakoor M, Vahedi A, Nematzadeh M, Tabari M. Post-heating flexural behavior of reinforced concrete beam with lap-spliced bar and feasibility of improving flexural performance by adding hybrid fibers. Structures: Elsevier; 2023. p. 965–82.
56. Nematzadeh M, Baradaran-Nasiri A, Hosseini M. Effect of pozzolans on mechanical behavior of recycled refractory brick concrete in fire. Struct Eng Mech Int'l J. 2019;72(3):339–54.

57. Jain A, Gupta R, Chaudhary S. Performance of self-compacting concrete comprising granite cutting waste as fine aggregate. Constr Build Mater. 2019;221:539–52.
58. Mukharjee BB, Barai SV. Influence of nano-silica on the properties of recycled aggregate concrete. Constr Build Mater. 2014;55:29–37.
59. Karimaei M, Dabbaghi F, Dehestani M, Rashidi M. Estimating compressive strength of concrete containing untreated coal waste aggregates using ultrasonic pulse velocity. Materials. 2021;14(3):647.
60. Velay-Lizancos M, Martinez-Lage I, Azenha M, Vázquez-Burgo P. Influence of temperature in the evolution of compressive strength and in its correlations with UPV in eco-concretes with recycled materials. Constr Build Mater. 2016;124:276–86.
61. Trtnik G, Kavčič F, Turk G. Prediction of concrete strength using ultrasonic pulse velocity and artificial neural networks. Ultrasonics. 2009;49(1):53–60.
62. Sadrmomtazi A, Gashti SH, Tahmouresi B. Residual strength and microstructure of fiber reinforced self-compacting concrete exposed to high temperatures. Constr Build Mater. 2020;230: 116969.
63. Rao A. Experimental investigation on use of recycled aggregates in mortar and concrete. In: Civil engineering, department of engineering. Kanpur: Indian Institute of Technology; 2005.
64. Pacheco-Torgal F, Miraldo S, Ding Y, Labrincha J. Targeting HPC with the help of nanoparticles: an overview. Constr Build Mater. 2013;38:365–70.
65. Hasan-Ghasemi A, Nematzadeh M. Tensile and compressive behavior of self-compacting concrete incorporating PET as fine aggregate substitution after thermal exposure: experiments and modeling. Constr Build Mater. 2021;289: 123067.
66. EN, 1992–1–2. design of concrete structures. Part 1–2: general rules—structural fire design," Eurocode 2, European Committee for Standardization, Brussels, Belgium, 2004.
67. Duarte G, Bravo M, de Brito J, Nobre J. Mechanical performance of shotcrete produced with recycled coarse aggregates from concrete. Constr Build Mater. 2019;210:696–708.
68. Wang Y, Liu F, Xu L, Zhao H. Effect of elevated temperatures and cooling methods on strength of concrete made with coarse and fine recycled concrete aggregates. Constr Build Mater. 2019;210:540–7.
69. ACI Committee 318-14. Building code requirements for structural concrete. Farmington Hills: American Concrete Institute; 2014.
70. Spanish code for structural concrete EHE. Real Decreto 2661/1998, Madrid; Dec 11; [in Spanish], 1998.
71. ACI 363. State-of-the-Art Report on High-Strength Concrete, American Concrete Institute, 1997.
72. Comité Euro-International du Béton. CEB-FIP model code 1990. London: Thomas Telford; 1993.
73. GB: 50010–2002. Chinese standard: code for design of concrete structures. Beijing (China): China building press, 2002, [in Chinese]
74. Brazilian association of technical standards NBR 6118. design of concrete structures, Rio de Janeiro, 2003, [in Portuguese]
75. Moghadam MA, Izadifard RA. Effects of steel and glass fibers on mechanical and durability properties of concrete exposed to high temperatures. Fire Saf J. 2020;113: 102978.
76. Nematzadeh M, Nazari A, Tayebi M. Post-fire impact behavior and durability of steel fiber-reinforced concrete containing blended cement–zeolite and recycled nylon granules as partial aggregate replacement. Arch Civil MechEng. 2021;22(1):5.